Multi-Metric Waveform Optimization for Multiple-Input Single-Output Joint Communication and Radar Sensing

Zhitong Ni, *Student Member, IEEE*, J. Andrew Zhang, *Senior Member, IEEE*, Kai Yang, *Member, IEEE*, Xiaojing Huang, *Senior Member, IEEE*, and Theodoros A. Tsiftsis, *Senior Member, IEEE*

***Abstract*—Joint communication and radar sensing (JCAS) integrates the two functions into one system, sharing one transmitted signal. In this paper, we investigate JCAS waveform optimization in communication-centric systems, where a base station (BS) detects radar targets and communicates with mobile users simultaneously. Different from existing works, we study multi-metric optimizations for a practical low-cost system and establish their connections. To relax the requirement of full-duplex technology, we add a single receive antenna for sensing at the BS, which is synchronized with and spatially separated from the JCAS transmit array. We first optimize precoders for communications and radar, individually. Then, we formulate a JCAS waveform optimization problem that constrains either mutual information (MI) or Cramér-Rao bound (CRB) of radar and maximizes the relaxed signal-to-interference-plus-noise rate (SINR) of communications. Exploiting the geometric characteristic of the relaxed SINR, we provide a closed-form solution under certain conditions and propose a numerical iteration algorithm that works in all situations. We also disclose the connections between optimizations with constraining MI and CRB, using numerical results. Finally, simulation results are provided and validate the proposed optimization solutions.**

***Index Terms*—Joint communication and radar sensing (JCAS), mobile networks, radar-communications, waveform optimization**

I. Introduction

Sharing many hardware and signal processing modules and transmitting one single signal, joint communication and radar sensing (JCAS) systems have shown great potential in many applications. One main application is for the fifth-generation (5G) cellular networks or beyond [**?**]. The 5G perceptive mobile network is proposed and aims to detect the surrounding environment using the communication links [**?**], [**?**]. The JCAS techniques will be the main feature in the sixth-generation (6G) cellular networks, dedicated to designing joint-function systems that use a single waveform to realize both communication and radar purposes [**?**]. JCAS systems have also attracted a lot of interest with applications in vehicular networks and self-driving [**?**], [**?**], [**?**], where signals used for communications between cars are also used for sensing the environment to detect objects and avoid collisions. For indoor environments, several works on passive WiFi sensing have been reported [**?**], [**?**], [**?**]. The underlying principle is to use the WiFi link to sense the object movements and human behaviour, which can be a promising technique for smart home applications. With sharing radar and communication functions, the JCAS devices can be smarter and more energy-efficient than conventional electronic devices. Moreover, with the deployment of a huge number of electronic devices in these future applications, JCAS techniques can reduce the hardware costs and power consumptions greatly [**?**].

A. Related Works

With most traditional hardware components replaced by digital processing modules, JCAS-enabled systems can reduce the number of connected devices and save the frequency resources [**?**], [**?**], [**?**]. To utilize the resources completely, most developed JCAS systems transmit single waveforms [**?**]. The resource utilization of the single waveform transmission schemes is highly efficient since the waveforms have dual functions that can be used for both communication and radar purposes. Such waveforms can be developed from classical radar waveforms [**?**], [**?**], [**?**] or conventional communication waveforms [**?**], [**?**].

Waveform optimization for JCAS has been reported in the literature. In [**?**], a multi-beam approach was proposed to flexibly generate JCAS sub-beams using analog antenna arrays. The optimization of the multi-beams was further investigated in [**?**]. This approach can adapt to varying channels but is suboptimal. In [**?**], the authors separated antenna arrays into two groups to realize dual-function JCAS systems. The radar waveform falls into the nullspace of the downlink channel, such that the interference between radar signals and communication

Manuscript received June 8, 2021; revised September 4, 2021, November 4, 2021, and November 22, 2021; accepted November 27, 2021. Date of publication; date of current version. This work is supported partially by China Scholarship Council and has also been partially supported by the Australian Research Council under grant No. DP210101411. *(Corresponding author: Kai Yang.)*

Z. Ni, K. Yang are with the School of Information and Electronics, Beijing Institute of Technology, Beijing, 100081, China. Z. Ni is also with the Global Big Data Technologies Centre, University of Technology Sydney, NSW, 2007, Australia (Emails: zhitong.ni@student.uts.edu.au, yangkai@ieee.org).

J. Andrew Zhang and X. Huang are with the Global Big Data Technologies Centre, University of Technology Sydney, NSW, 2007, Australia (Emails: Andrew.Zhang@uts.edu.au, xiaojing.huang@uts.edu.au).

T. A. Tsiftsis is with the School of Intelligent Systems Science and Engineering, Jinan University, Zhuhai 519070, China, and also with the School of Science, University of Thessaly, Lamia 35131, Greece (email: tsiftsis@ieee.org).

signals can be minimized. A multi-objective function was further applied to trade off the similarity between the generated waveform and the desired one in [**?**]. The multi-objective function in [**?**] is a weighted sum of two individual optimal waveforms. In [**?**], the authors maximized the radar signal-to-interference-plus-noise ratio (SINR) with a given specific capacity of communication channels. The work in [**?**], [**?**] further introduced a sub-sampling matrix for radar as an objective function of the optimization. Most of these existing works either optimized one-side (radar/communication) performance with constraining the other side (communication/radar) [**?**], [**?**], [**?**], [**?**] or adopted a weighted-sum solution to optimize joint metrics with constraining the power [**?**], [**?**], [**?**]. Except those two main-stream methodologies, there are also some works that design the desired beam directions for both radar and communications, and embed the information on the sidelobes of radar beams [**?**], [**?**]. In this paper, we would like to regulate both radar and communications, so that they each can achieve a required performance threshold.

When optimizing JCAS waveforms, different performance metrics for both communications and radar sensing can be used. The metrics for multiuser communication systems include multiuser interference (MUI) [**?**], [**?**] and effective channel gain (ECG) [**?**]. The MUI tolerance was analyzed for multi-input-multi-output orthogonal-frequency-division-multiplexing (MIMO-OFDM) JCAS systems in [**?**], using the interleaved signal model in [**?**]. The individual optimal communication waveform in [**?**] is also based on minimizing the MUI. However, simply minimizing MUI can cause the JCAS signals to fall into the nullspace of individual communication signals and result in a low sum rate. To tackle this issue, the authors in [**?**] introduced an expected diagonal matrix that requires a constellation symbol matrix (CSM). As for radar sensing, typically considered performance metrics include mutual information (MI) [**?**], [**?**], Cramér-Rao bound (CRB) [**?**], [**?**], and minimum mean-squared error (MMSE) [**?**]. In [**?**], MI for an OFDM JCAS system was studied, and the power allocation on subcarriers was investigated by maximizing the weighted sum of the MI of radar and the MI of communication. In [**?**], the authors developed an MI measure that jointly optimizes the performance of radar and communication systems that overlap in the same frequency band. The CRB and MMSE are also commonly-used metrics for waveform optimization. In [**?**], the authors derived the performance bounds for a single antenna system. In [**?**], the authors derived performance bounds for the radar estimation rate based on MMSE estimation bounds.

B. Motivations and Contributions

This paper develops waveform optimization approaches for OFDM JCAS systems and aims to establish connections between different commonly-used metrics. Firstly, we consider a practical JCAS system of deployment, using a single dedicated receive antenna for sensing. JCAS systems, particularly those underlying communication signals, confront the major challenge of full-duplex, that is, transmitting and receiving at the same time using the same frequency channel [**?**]. Solutions bypassing full-duplex requirements were discussed in [**?**], [**?**]. Here, we adopt a single receive antenna dedicated to radar sensing, which is a low-cost and practical solution at the moment. Due to the use of a frequency-modulated continuous-wave signal, the sensing antenna is widely separated from the transmit array, and hence can perfectly retrieve the receive echo signals for sensing without short range leakage (SRL) effects [**?**], [**?**]. Secondly, there are not many papers that conduct parallel comparisons between multiple performance metrics in JCAS systems so far. We aim to optimize the precoder of communications with constraining one of the radar performance metrics including CRB and MI. We formulate the optimization problems for both MI and CRB of radar under the same communication framework. In addition to providing closed-form solutions to the optimization problems, we are able to establish and observe connections between using MI and CRB as optimization metrics.

The main contributions of this paper are summarized as follows.

- We derive multiple metrics, including a novel relaxed SINR for communications, and MI and CRB for radar sensing, in an OFDM-based JCAS system. In the adopted system, bypassing the full-duplex requirement, one single-antenna sensing receiver is used for collecting the signals reflected from targets.
- We propose the relaxed SINR by summing the traditional ones for all users. Instead of using the conventional semi-definite relaxation (SDR) method, we analyze the geometric characteristic of the proposed relaxed SINR. Due to its hyperbolic characteristic, we can obtain the closed-form solution of the precoder to the relaxed SINR optimization problem. Additionally, we can obtain the precoder directly without the requirement of transforming the covariance matrix to the precoder.
- We derive multiple metrics, including MI and CRB, for radar and optimize the precoders using these metrics. We also show that MI focuses on the accuracy of the whole channel vectors, while the CRB is biased on the accuracy of the derivatives of the channel vectors with respect to different parameters.
- We formulate two JCAS precoding optimization problems with constraints on the users' achieved SINRs and the achieved MI/CRB of radar. We provide both closed-form solutions under certain conditions and numerical iteration algorithms. We also show the JCAS performance gaps between those two different radar constraints via numerical results.

Notations: $\mathbf{a}$ denotes a vector, $\mathbf{A}$ denotes a matrix, italic English letters like N and lower-case Greek letters α are a scalar. $|\mathbf{A}|, \mathbf{A}^T, \mathbf{A}^H, \mathbf{A}^*$, and $\mathbf{A}^\dagger$ represent determinant value, transpose, conjugate transpose, conjugate, and pseudo inverse, respectively. We use $\mathrm{diag}(\mathbf{a})$ to denote a diagonal matrix with

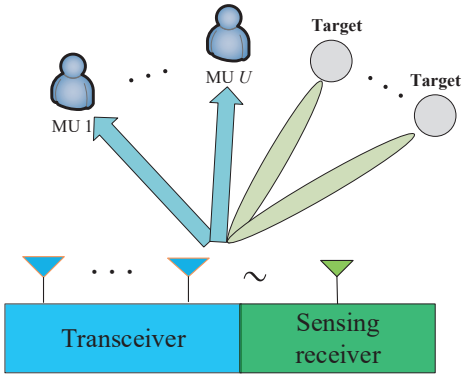

Fig. 1. Illustration of JCAS systems with downlink sensing. The BS uses a single-antenna receiver dedicated for sensing the reflected downlink signals.

diagonal entries being the entries of $\mathbf{a}$ and $\mathrm{Tr}(\mathbf{A})$ to denote the trace of a square matrix. $\|\mathbf{A}\|_F$ and $[\mathbf{A}]_N$ represent the Frobenius norm and the Nth column of a matrix, respectively.

II. System and Channel Models

We consider an OFDM-based JCAS system supporting multiuser communications, as well as active downlink sensing. As shown in Fig. 1, the sensing is conducted at the BS, where an $N \times 1$ uniform linear array (ULA) is employed for transmitting communication data blocks. Since the full-duplex technologies are not mature yet, we consider a low-cost alternative setup, where a single antenna, sufficiently separated from and synchronized with the transmit array, is used for solely collecting the reflected signals and sensing. This antenna can be co-located with the transmit array or geometrically separated. In the former, SRL signals from the transmitter is largely separated and can be simply removed as they are known at the receiver. In the latter, in terms of sensing, it is equivalent to a bi-static radar. For both cases, the system is equivalent to a multi-input-single-output (MISO) system for sensing. Hence, sensing parameters except for the angle-of-arrivals (AoAs) can be effectively estimated by using the received signals at the BS. The role of AoAs in localization can be substituted by angle-of-departures (AoDs) in our considered system.

The OFDM signal consists of K subcarriers with the subcarrier interval $\Delta f = 1/T$, where T is the length of one OFDM symbol exclusive of the cyclic prefix (CP) of length T_{C}. Let $\mathbf{s}[k,m]$ denote a $U\times 1$ data symbol vector on subcarrier k of the mth time slot. A digital precoder with the dimension of $N\times U$, $\mathbf{P}[k,m]$, is applied to $\mathbf{s}[k,m]$, such that $\|\mathbf{P}[k,m]\|_F^2 \le U$. The precoded data symbol vector is written as

$$\begin{aligned}&\mathbf{x}[k,m] = \mathbf{P}[k,m]\mathbf{s}[k,m],\\ &k \in \{0,\cdots,K-1\}, m \in \{0,\cdots,M-1\}.\end{aligned} \tag{1}$$

An inverse fast Fourier transform (IFFT) across the frequency band is then applied to the elements of $\mathbf{x}[k,m]$ from $k=0$ to $k=K-1$ and transforms signals into time domain. The time-domain signals are transmitted by the $N\times 1$ ULA.

The BS conducts downlink communications with U mobile users (MUs) that may also become part of the targets in sensing. Each user has a single receive antenna. The transmitted signals go through a finite-scatter channel model [**?**], given by

$$\mathbf{h}_u^{\mathrm{C}}[k,m] = \sum_{l_u=1}^{L_u} \beta_{l_u}\mathbf{a}(\Phi_{l_u})e^{-j2\pi k\frac{\tau_{l_u}}{T}}e^{j2\pi m f_{d,l_u}(T+T_c)}, \tag{2}$$

where β_{l_u} is the channel gain of the l_uth path between BS and MU u, $\Phi_{l_u} = \pi\sin(\varphi_{l_u})$ is the equivalent AoD with φ_{l_u} being the actual AoD, $\mathbf{a}(\cdot)$ is an $N\times 1$ normalized ULA array response vector, τ_{l_u} is the time delay of the lth path of user u, f_{d,l_u} is the Doppler frequency of the lth path of user u, and T_c is the duration of a CP. We can use traditional least square (LS) method to estimate the channel model. We assume that $f_{d,l_u}(T+T_c)$ is small enough, such that the term of $e^{j2\pi m f_{d,l_u}(T+T_c)}$ can be regarded unchanged and can be absorbed into the coefficients β_{l_u} from $m=0$ to $m=M-1$. Thus, the channel model becomes invariant to the time slot. Let us send a data block $\mathbf{S}[k] = \big[\mathbf{s}[k,0],\cdots,\mathbf{s}[k,M-1]\big]$ of length M at the baseband of BS. We assume the data symbols are statistically independent, i.e., $\mathbb{E}(\mathbf{S}[k]\mathbf{S}^H[k]) = P\mathbf{I}$, where P is the transmit power. The received signal for each user is sampled at the interval of T/K and converted to the frequency domain using K-point FFTs after removing CP. We assemble a limited number of M time slots. The received data symbol of the uth user is

$$\mathbf{r}_u[k] = (\mathbf{h}_u^{\mathrm{C}}[k])^H\mathbf{P}[k]\mathbf{S}[k] + \mathbf{n}_u^{\mathrm{C}}[k], \tag{3}$$

where $\mathbf{n}_u^{\mathrm{C}}[k]$ is a complex AWGN vector with zero mean and covariance matrix of $\sigma_{\mathrm{C}}^2\mathbf{I}_M$, $\mathbf{P}[k]$ is the precoder during the first M time slots, and $\mathbf{h}_u^{\mathrm{C}}[k]$ equals $\mathbf{h}_u^{\mathrm{C}}[k,0]$.

Meanwhile, the BS utilizes the single-antenna receiver as in Fig. 1 to perform radar sensing. The transmitted signals from N antennas impinge on L targets with the time delays of $\{\tau_l\}_{l=1}^L$. We still omit the Doppler term and write the sensing channel as

$$\mathbf{h}^{\mathrm{S}}[k] = \sum_{l=1}^{L}\alpha_l\mathbf{a}(\Omega_l)e^{-j2\pi k\frac{\tau_l}{T}} = \mathbf{A}\mathbf{\Psi}\mathbf{\Phi}[k]\mathbf{1}, \tag{4}$$

where α_l is the path loss coming from the lth target, $\Omega_l = \pi\sin(\omega_l)$ is the equivalent AoD with ω_l being the AoD of targets, τ_l is the time delay of the targets, $\mathbf{A} = [\mathbf{a}(\Omega_1),\cdots,\mathbf{a}(\Omega_L)]$, $\mathbf{\Psi} = \mathrm{diag}(\alpha_1,\cdots,\alpha_L)$, $\mathbf{\Phi}[k] = \mathrm{diag}([e^{-j2\pi k\frac{\tau_1}{T}},\cdots,e^{-j2\pi k\frac{\tau_L}{T}}])$, and $\mathbf{1}$ is a vector with all entries being 1s. We assume that the entries of the radar channel vectors are independent and identically distributed (i.i.d.). The received frequency-domain signal at the sensing receiver of the BS is written as

$$\mathbf{r}[k] = (\mathbf{h}^{\mathrm{S}}[k])^H\mathbf{P}[k]\mathbf{S}[k] + \mathbf{n}^{\mathrm{S}}[k], \tag{5}$$

where $\mathbf{n}^{\mathrm{S}}[k]$ is a complex additive-white-Gaussian-noise (AWGN) vector at the sensing receiver, and it has zero mean and covariance matrix of $\sigma^2\mathbf{I}_M$.

III. Individual Performance Metrics

In this section, we derive the performance metrics for communications and sensing individually. For communications, we consider the SINR metric. Due to the non-convex nature of the SINR expression, we can use the traditional semi-definite relaxation (SDR) technique [**?**] to relax SINR. By fixing the SINR thresholds to be the same among users, we also propose a novel relaxed SINR that has a quadratic form. For radar sensing, we consider two different metrics, MI and CRB, and aim to disclose the links between these metrics in the JCAS design.

A. Metrics for Communications

The SINR is one of the main performance metrics considered in communications, especially in multiuser systems. For the studied system, the SINR on the kth subcarrier of the uth user is given by

$$\mathrm{SINR}_{k,u} = \frac{\frac{P}{U}|(\mathbf{h}_u^{\mathrm{C}}[k])^H \mathbf{p}_u[k]|^2}{\frac{P}{U}\sum\limits_{v\neq u}|(\mathbf{h}_u^{\mathrm{C}}[k])^H \mathbf{p}_v[k]|^2 + \sigma_{\mathrm{C}}^2}, \tag{6}$$

where $\mathbf{p}_u[k]$ is the uth column of $\mathbf{P}[k]$. The SINR has a non-convex form and is difficult to optimize, especially when joint optimization in JCAS is required. By letting

$$\mathbf{H}_{k,u} = \mathbf{h}_u^{\mathrm{C}}[k](\mathbf{h}_u^{\mathrm{C}}[k])^H, \mathbf{Q}_{k,u} = \mathbf{p}_u[k]\mathbf{p}_u^H[k], \tag{7}$$

we can use the traditional SDR technique [**?**] to relax the SINR into the following form,

$$R_{k,u} = \mathrm{Tr}(\mathbf{Q}_{k,u}\mathbf{H}_{k,u}) - \gamma_{k,u}\left(\sum_{v\neq u}\mathrm{Tr}(\mathbf{Q}_{k,v}\mathbf{H}_{k,u}) + \frac{\sigma_{\mathrm{C}}^2 U}{P}\right), \tag{8}$$

where $\gamma_{k,u}$ is a given threshold, such that $\mathrm{SINR}_{k,u} \geq \gamma_{k,u}$, which is equivalent to $R_{k,u} \geq 0$. According to [**?**], we can prove that $R_{k,u}+\gamma_{k,u}$ can be seen as a lower bound of $\mathrm{SINR}_{k,u}$ at high SNRs.

Proof. Dividing $R_{k,u}$ by $\left(\sum\limits_{v\neq u}\mathrm{Tr}(\mathbf{Q}_{k,v}\mathbf{H}_{k,u}) + \frac{\sigma_{\mathrm{C}}^2 U}{P}\right)$, we have

$$\frac{R_{k,u}}{\sum\limits_{v\neq u}\mathrm{Tr}(\mathbf{Q}_{k,v}\mathbf{H}_{k,u}) + \frac{\sigma_{\mathrm{C}}^2 U}{P}} = \mathrm{SINR}_{k,u} - \gamma_{k,u}.$$

Note that $\sum\limits_{v\neq u}\mathrm{Tr}(\mathbf{Q}_{k,v}\mathbf{H}_{k,u})$ denotes the MUI of the system. Generally, we can regulate the power of precoder, such that it is smaller than 1. At high SNRs, the term of $\frac{\sigma_{\mathrm{C}}^2 U}{P}$ can be seen as zero. Then, we have $\mathrm{SINR}_{k,u} - \gamma_{k,u} \geq R_{k,u}$. Hence, at high SNRs, $R_{k,u} + \gamma_{k,u}$ can be seen as a lower bound of $\mathrm{SINR}_{k,u}$. □

The relaxed SINR, $R_{k,u}$, can be solved using the standard semi-definite programming (SDP). Nevertheless, the obtained ideal $\mathbf{Q}_{k,u}$ always has a high rank while the practical $\mathbf{Q}_{k,u}$ is $\mathbf{p}_u[k]\mathbf{p}_u^H[k]$ and only has a rank of 1. Some papers use rank reduction approaches [**?**] to force $\mathbf{Q}_{k,u}$'s rank to be 1, but these approaches will cause distortion errors between the ideal $\mathbf{Q}_{k,u}$ and the rank-reduced $\mathbf{Q}_{k,u}$. For this problem, we propose a novel metric that can use $\mathbf{p}_u[k]$ instead of $\mathbf{Q}_{k,u}$ to optimize the sum of $R_{k,u}$.

As detailed in Appendix **??**, we can rewrite $R_{k,u}$ into the following form,

$$\begin{aligned} R_{k,u} =& (\mathbf{p}_u^H[k]\mathbf{H}_{k,u}\mathbf{p}_u[k]) \\ &- \gamma_{k,u}\left(\sum_{v\neq u}(\mathbf{p}_v^H[k]\mathbf{H}_{k,u}\mathbf{p}_v[k]) + \frac{\sigma_{\mathrm{C}}^2 U}{P}\right). \end{aligned} \tag{9}$$

Now, letting $\gamma_{k,u}$ be invariant to u, we develop a metric, $R_k = \sum\limits_{u=1}^{U} R_{k,u}$, which can be represented as

$$\begin{aligned} & R_k \\ =& \sum_{u=1}^{U}(\mathbf{p}_u^H[k]\mathbf{H}_{k,u}\mathbf{p}_u[k]) \\ &- \gamma_k\left(\sum_{u=1}^{U}\sum_{v\neq u}(\mathbf{p}_v^H[k]\mathbf{H}_{k,u}\mathbf{p}_v[k]) + \frac{\sigma_{\mathrm{C}}^2 U^2}{P}\right) \\ =& \sum_{u=1}^{U}(\mathbf{p}_u^H[k]\mathbf{H}_{k,u}\mathbf{p}_u[k]) \\ &- \gamma_k\left(\sum_{u=1}^{U}\sum_{v\neq u}(\mathbf{p}_u^H[k]\mathbf{H}_{k,v}\mathbf{p}_u[k]) + \frac{\sigma_{\mathrm{C}}^2 U^2}{P}\right) \\ =& \sum_{u=1}^{U}\left(\mathbf{p}_u^H[k]\left(\mathbf{H}_{k,u} - \gamma_k\sum_{v\neq u}\mathbf{H}_{k,v}\right)\mathbf{p}_u[k]\right) - \gamma_k\frac{\sigma_{\mathrm{C}}^2 U^2}{P}. \end{aligned} \tag{10}$$

As mentioned above, $R_{k,u}+\gamma_{k,u}$ is a lower bound of $\mathrm{SINR}_{k,u}$. Similarly, $R_k + \gamma_k$ can be seen as the lower bound of the average SINR for all users. Since γ_k is a fixed value, we only need to maximize R_k instead. We denote $\sum\limits_{u=1}^{U}\mathrm{SINR}_{k,u}/U$ as the average SINR on subcarrier k. By maximizing R_k under the constraint of $R_{k,u} \geq 0$, we can guarantee that the average SINR is maximized, while each user meet the lowest SINR requirement. Let $\mathbf{C}_{k,u} = \mathbf{H}_{k,u} - \gamma_k\sum\limits_{v\neq u}\mathbf{H}_{k,v}$. We note that R_k is a quadratic form. More specifically, when $\mathbf{p}_u[k]$ is a real vector of dimension two, R_k is a hyperbola curve, and when $\mathbf{p}_u[k]$ is a real vector of dimension three, R_k is a saddle surface. Even though the reformulated R_k is still not a convex function, we can exploit the geometric characteristic of hyperbola curve to obtain its optimal value. The individual precoding optimization problem for communications can hence

be formulated as

$$\arg\max_{\mathbf{P}[k]} R_k = -\gamma_k \frac{\sigma_C^2 U^2}{P} + \sum_{u=1}^{U} \mathbf{p}_u^H[k]\mathbf{C}_{k,u}\mathbf{p}_u[k]$$
$$\text{s.t.} \|\mathbf{P}[k]\|_F^2 \le U, R_{k,u} \ge 0. \tag{11}$$

We note that, in most cases, only the first eigenvalue of $\mathbf{C}_{k,u}$ is positive. This is resulted from the low correlation among the communication channel vectors. Considering a specific case when the communication channel vectors are orthogonal with one another, they become the eigenvectors of $\mathbf{C}_{k,u}$ and the eigenvalues of $\mathbf{C}_{k,u}$ are $\|\mathbf{h}_u^{\mathrm{C}}[k]\|^2$ and $-\|\mathbf{h}_v^{\mathrm{C}}[k]\|^2, \forall v \neq u$. When the channel vectors are statistically independent, it is still held that only the first eigenvalue is positive because the channel vector of $\mathbf{h}_u^{\mathrm{C}}[k]$ has little projection value on the other channel vectors of $\mathbf{h}_v^{\mathrm{C}}[k], \forall v \neq u$.

B. MI for Radar Sensing

MI is a widely-used metric in both radar and communication systems. For radar, maximizing MI enables the maximization of information/entropy on targets in the received signal. Since the channel vector is the main concern for the radar system, MI determines how much entropy can be transformed to the receiver side. For radar, the transmitted symbols are already known at the receiver side. Hence, the MI is generally written in a conditional form. The conditional MI is defined as the entropy between the channel and the received signals with a given transmit symbol. Following the derivations in [**?**], the MI between the channel vectors and the received signals for radar sensing can be represented as

$$\begin{aligned}\mathrm{MI} =& I(\mathbf{h}^{\mathrm{S}}[k]; \mathbf{r}[k]|\mathbf{S}[k]) \\ =& \log_2\left|\sigma^{-2} P \mathbf{h}^{\mathrm{S}}[k]^H \mathbf{P}[k]\mathbf{P}^H[k]\mathbf{h}^{\mathrm{S}}[k] + 1\right|. \end{aligned} \tag{12}$$

It is clear that the optimal $\mathbf{P}[k]$ should have only one dimension spanned by $\mathbf{h}^{\mathrm{S}}[k]$. Since $\mathbf{P}[k]$ has U columns, $\mathbf{P}[k]$ can be rewritten as $\mathbf{P}[k] = \mathbf{h}^{\mathrm{S}}[k]\mathbf{\Lambda}[k]$, where $\mathbf{\Lambda}[k]$ is a $1 \times U$ vector, such that $\|\mathbf{h}^{\mathrm{S}}[k]\mathbf{\Lambda}[k]\|_F^2 = U$. However, the obtained precoder has only U variables in $\mathbf{\Lambda}[k]$. For JCAS optimization, the obtained solution has a limited degree of freedom and cannot achieve a flexible tradeoff between radar and communication performances, as will be investigated in section IV. To get more insights from the MI expression, we decompose $\mathbf{P}[k]$ into the following form,

$$\mathbf{P}[k] = \mathbf{h}^{\mathrm{S}}[k]\mathbf{\Lambda}[k] + \mathbf{N}[k], \tag{13}$$

where $\mathbf{\Lambda}[k] = (\mathbf{h}^{\mathrm{S}}[k])^{\dagger}\mathbf{P}[k]$ and $\mathbf{N} = \mathbf{P} - \mathbf{h}^{\mathrm{S}}\mathbf{\Lambda}$. It is decomposed in this way such that $\mathbf{h}^{\mathrm{S}}[k]\mathbf{\Lambda}[k]$ contains the component that can change the value of MI, and $\mathbf{N}[k]$ is a matrix with columns in the nullspace of $\mathbf{h}^{\mathrm{S}}[k]\mathbf{\Lambda}[k]$. Thus, the columns of $\mathbf{N}[k]$ are orthogonal with those of $\mathbf{h}^{\mathrm{S}}[k]\mathbf{\Lambda}[k]$. Substituting (13) into MI of (12), we have

$$\begin{aligned}&\mathrm{MI} \\ =& \log_2\left|\sigma^{-2} P \mathbf{h}^{\mathrm{S}}[k]^H (\mathbf{h}^{\mathrm{S}}[k]\mathbf{\Lambda}[k] + \mathbf{N}[k]) \times \right. \\ & \left. (\mathbf{h}^{\mathrm{S}}[k]\mathbf{\Lambda}[k] + \mathbf{N}[k])^H \mathbf{h}^{\mathrm{S}}[k] + 1\right| \\ =& \log_2\left|\sigma^{-2} P \mathbf{h}^{\mathrm{S}}[k]^H (\mathbf{h}^{\mathrm{S}}[k]\mathbf{\Lambda}[k])(\mathbf{h}^{\mathrm{S}}[k]\mathbf{\Lambda}[k])^H \mathbf{h}^{\mathrm{S}}[k] + 1\right| \\ =& \log_2\left|\sigma^{-2} P h_k \lambda_k + 1\right| \le \max(\mathrm{MI}), \end{aligned} \tag{14}$$

where $h_k = \|\mathbf{h}^{\mathrm{S}}[k]\|_F^4$, $\lambda_k = \mathbf{\Lambda}[k]\mathbf{\Lambda}^H[k]$.

C. CRB for Radar Sensing

CRB is a theoretical lower bound of the estimation errors of parameters. The minimization of CRB does not directly influence the actual estimation errors, since it is a lower bound, but it can reflect the potential gaps between the actual estimation methods and the ideal optimal one. The CRB has many different forms, depending on the formulation of the channel parameters [**?**]. In our considered broadband MISO systems, we mainly study the estimation for delays, complex gains, and AoDs of the targets, exclusive of the Doppler frequencies. For convenience, we represent all parameters collectively using one common real-valued vector $\mathbf{\Theta} = \left[\mathrm{Re}[\alpha_1, \cdots, \alpha_L], \mathrm{Im}[\alpha_1, \cdots, \alpha_L], \tau_1, \cdots, \tau_L, \Omega_1, \cdots, \Omega_L\right]^T$. It is noted that there are $4L$ parameters in total. Hence, the received signal vector is a function of $4L$ variables.

The CRB matrix, denoted as $\mathbf{B}$, contains all lower bounds of the estimation errors [**?**]. To jointly evaluating these bounds, we can count the total CRB as the Frobenius norm of $\mathbf{B}$. The CRB matrix is the inverse of the Fisher information matrix (FIM), i.e., $\mathbf{B} = \mathbf{F}^{-1}$. Referring to the derivations of [**?**] and using the so-called *DOD/DOA Model* defined in [**?**], we obtain our corresponding FIM as

$$\mathbf{F} = \begin{bmatrix} \mathrm{Re}[\mathbf{F}_1] & -\mathrm{Im}[\mathbf{F}_1] & \mathrm{Re}[\mathbf{F}_2] & \mathrm{Re}[\mathbf{F}_3] \\ \mathrm{Im}[\mathbf{F}_1] & \mathrm{Re}[\mathbf{F}_1] & \mathrm{Im}[\mathbf{F}_2] & \mathrm{Im}[\mathbf{F}_3] \\ \mathrm{Re}[\mathbf{F}_2^T] & \mathrm{Im}[\mathbf{F}_2^T] & \mathrm{Re}[\mathbf{F}_4] & \mathrm{Re}[\mathbf{F}_5] \\ \mathrm{Re}[\mathbf{F}_3^T] & \mathrm{Im}[\mathbf{F}_3^T] & \mathrm{Re}[\mathbf{F}_5^T] & \mathrm{Re}[\mathbf{F}_6] \end{bmatrix}, \tag{15}$$

where the expressions of $\mathbf{F}_1$ to $\mathbf{F}_6$ are provided in Appendix **??**. The derivation can be referred to [**?**].

From Appendix **??**, we see that the FIM matrix depends on the covariance matrix, $\mathbf{Q}[k] = \mathbf{P}[k]\mathbf{P}^H[k]$, only. Therefore, the CRB-based optimization problem is equivalent to optimizing $\mathbf{Q}[k]$. We aim to minimize the largest eigenvalue of the CRB matrix as in [**?**]. Minimizing the largest eigenvalue of the CRB matrix is equivalent to maximizing the smallest eigenvalue of the FIM. The waveform optimization under the eigen-optimization criterion can be directly formulated as an SDP,

$$\begin{aligned}&\arg\min_{\mathbf{Q}[k]} -t \\ &\text{s.t.} \mathbf{F} \succeq t\mathbf{I}, \mathbf{Q}[k] \succeq \mathbf{0}, \mathrm{Tr}(\mathbf{Q}[k]) \le P, \end{aligned} \tag{16}$$

where t is an auxiliary variable.

When optimizing $\mathbf{F}$ as a whole, we note that it is difficult not to use SDPs. After obtaining $\mathbf{Q}[k]$ via SDPs, we still need to obtain $\mathbf{P}[k]$. We introduce the rank reduction method in [**?**] to obtain $\mathbf{P}[k]$ from the rank reduced $\mathbf{Q}[k]$. This would result in errors for $\mathbf{Q}[k]$ and cannot guarantee the optimality of $\mathbf{P}[k]$. Fortunately, we can prove that the $\mathbf{P}[k]$ can be obtained perfectly from the optimal $\mathbf{Q}[k]$ when $\mathbf{F}$ equals $\mathrm{Re}[\mathbf{F}_4]$, $\mathrm{Re}[\mathbf{F}_6]$, or

$\mathbf{F}_1$. This means that the CRB of the estimate for one parameter is optimized when other parameters are fixed. The proof is provided in Appendix **??**.

Remark 1: To this end, we have introduced all required communication and radar metrics, two relaxed SINR expressions for communications, and MI and CRB for radar. The proposed novel relaxed SINR is the sum of all users' relaxed SINRs and makes their thresholds to be the same. The proposed communication metric has two main advantages. Firstly, we can avoid using SDP methods to solve the optimization problem, and obtain $\mathbf{P}[k]$ directly without the requirement of transforming $\mathbf{Q}[k]$ into $\mathbf{P}[k]$. Secondly, we can get a clear view of the geometric property of the proposed metric. By using its unique geometric property, we can obtain the closed-form solution for the JCAS optimization problems.

Remark 2: Intuitively, we can see the following connections between MI and CRB metrics. Referring to the optimal MI radar precoder, $\mathbf{h}^{\mathrm{S}}[k]\mathbf{\Lambda}[k]$, we can observe that it only has a rank of one while the optimal CRB precoder has a rank of L. For the CRB of delays, angles, and complex path gains, $\mathbf{F}$ is equal to $\mathrm{Re}[\mathbf{F}_4]$, $\mathrm{Re}[\mathbf{F}_6]$, and $\mathbf{F}_1$, respectively. As can be seen from Appendix **??** and **??**, the optimal $\mathbf{P}[k]$ corresponding to these CRBs equal $\mathbf{A}[\bar{\mathbf{B}}[k]]^{\frac{1}{2}}_{1:L,1:L}$, $\dot{\mathbf{A}}[\bar{\mathbf{B}}[k]]^{\frac{1}{2}}_{1:L,1:L}$, and the right singular vectors of $\mathbf{\Phi}[k]\mathbf{A}$, respectively. Apparently, the two different radar metrics, MI and CRB, have different focuses on the system designs. The optimal MI solution tends to maximize the received power and the channel information, whereas the optimal CRB solutions minimize the variance of the estimation errors for different sensing parameters, based on different partial matrices of the FIM, which are the derivatives of the channel vectors with respect to different parameters. We can compare these two metrics in parallel via simulations, as will be detailed in section **??**.

IV. MI Constrained JCAS Waveform Optimization

We have introduced all required radar and communication metrics. In this section, we aim to optimize the communication metric with constraining the MI of radar. We will provide both a closed-form optimal solution under certain conditions and a more general numerical iteration algorithm.

A. Closed-Form Solution

The proposed relaxed SINR, $R_k + \gamma_k$, is a lower bound of the SINR. Note that $R_k + \gamma_k \frac{\sigma_{\mathrm{C}}^2 U^2}{P}$ is a quadratic form that is symmetric to the original point. The symmetric property makes it easy to obtain our following derivations. Hence, we define J_k as $R_k + \gamma_k \frac{\sigma_{\mathrm{C}}^2 U^2}{P}$ and maximize J_k instead of R_k. The MI-constrained JCAS optimization problem is formulated as

$$\begin{aligned}\arg\max_{\mathbf{P}[k]} J_k = R_k + \gamma_k \frac{\sigma_{\mathrm{C}}^2 U^2}{P} = \sum_{u=1}^{U} \mathbf{p}_u[k]^H \mathbf{C}_{k,u} \mathbf{p}_u[k] \\ \text{s.t.} \|\mathbf{P}[k]\|_F^2 \le U, \mathrm{MI} \ge I_0, R_{k,u} \ge 0, \forall u \in \{1, \cdots, U\},\end{aligned} \tag{17}$$

where the power of the precoder is normalized to be no greater than U, the MI of radar is restricted to be no smaller than a given threshold, i.e., I_0, and the relaxed SINR for communications, $R_{k,u}$, is no smaller than 0, which means that the SINR of the uth user is no smaller than the threshold. It is noted that all variables have an index of k. For notational simplicity, we omit the index k in the following of this subsection.

Using the decomposition of $\mathbf{P}$ in (13) and the MI expression in (14), we can rewrite the second constraint of (17) into a simpler form,

$$\lambda = \|\mathbf{\Lambda}\|_F^2 \ge \frac{\sigma^2(2^{I_0} - 1)}{Ph}. \tag{18}$$

Note that this form is equivalent to $\mathrm{MI} \ge I_0$. Let $\mathbf{p}_u = \mathbf{v}_u + \mathbf{w}_u$, where $\mathbf{v}_u$ denotes the uth column of $\mathbf{h}^{\mathrm{S}}\mathbf{\Lambda}$ and $\mathbf{w}_u$ is the uth column of $\mathbf{N}$ that is orthogonal to $\mathbf{v}_u$. With a given $\mathbf{p}_u$, $\mathbf{v}_u$ is given by $\frac{\mathbf{h}^{\mathrm{S}}(\mathbf{h}^{\mathrm{S}})^H \mathbf{p}_u}{\|\mathbf{h}^{\mathrm{S}}\|_F^2}$, and $\mathbf{w}_u$ is given by $\mathbf{p}_u - \mathbf{v}_u$.

The MI constrained problem is now simplified as

$$\begin{aligned}\arg\max_{\mathbf{p}_u} \quad & J \\ \text{s.t.} \|\mathbf{P}\|_F^2 \le U, \|\mathbf{\Lambda}\|_F^2 \ge \frac{\sigma^2(2^{I_0} - 1)}{Ph}, & R_u \ge 0, \forall u \in \{1, \cdots, U\}.\end{aligned} \tag{19}$$

Now, we provide the closed-form solution to (17), presented in Lemma 1 and Theorem 1.

Lemma 1. *The maximal value of J is obtained when $\mathbf{p}_u$ is on the surface of the constraints, i.e., $\sum_{u=1}^{U} \|\mathbf{p}_u\|_F^2 = U$ or $\|\mathbf{\Lambda}\|_F^2 = \frac{\sigma^2(2^{I_0}-1)}{Ph}$, or $R_u = 0$.*

Proof. The proof is shown in Appendix **??**. □

According to Lemma 1, we obtain an important theorem that directly leads to the closed-form solution of $\mathbf{p}_u$, which is illustrated as follows.

Theorem 1. *Let us denote the constraint equations as $\|\mathbf{P}\|_F^2 = U$, $\mathrm{MI} = I_0$, and $R_u = 0, \forall u$. The corresponding constraint inequations are $\|\mathbf{P}\|_F^2 \le U$, $\mathrm{MI} \ge I_0$, and $R_u \ge 0, \forall u$. The closed-form solution of the precoding vector has the form of $\mathbf{p}_u = \sum_{i=1}^{C} a_{u,i}\mathbf{c}_{u,i}$, where $a_{u,i}$ are non-zero scaling factors, C is the number of positive eigenvalues in $\mathbf{C}_u$, and $\mathbf{c}_{u,i}$ is the i-th eigenvector of $\mathbf{C}_u$. The closed-form solution exists only when it satisfies $\|\mathbf{P}\|_F^2 \le U$ and $\mathrm{MI} \ge I_0$ and $R_u \ge 0$ and $\{\|\mathbf{P}\|_F^2 = U$ or $\mathrm{MI} = I_0$ or $R_u = 0\}$.*

Proof. The proof is shown in Appendix **??**. □

The closed-form solution can be obtained when $a_{u,i}$ exists. The existence of the closed-form solution depends on the intersection of two spaces. One space is formed by constraints. The other is spanned by $\mathbf{c}_{u,i}, i \ge C$. If there is no intersection between these two spaces, the closed-form solution does not exist. Otherwise, the closed-form solution is given by the linear expression of $\mathbf{c}_{u,i}, i \ge C$. From the illustration in Fig. 2, we

can see that the intersection of the two spaces may be empty. Hence, in general cases, whenever the intersection is empty or not, we will propose an iterative algorithm to solve the problem.

In general cases, we can obtain the following corollary.

Corollary 1. *The optimal point of* $\mathbf{P}$ *is on the tangent plane of* $J(\mathbf{P}) = J_0$ *with* J_0 *being the maximal value.*

Proof. The proof is shown in Appendix **??**. □

B. Iterative Solution

Next, we propose an iteration algorithm based on the Newton's method [**?**] when the closed-form solution cannot be obtained. According to the proof of Lemma 1, we can make $\mathbf{p}_u$ reach one surface of the constraints. Fig. 2 explains how our proposed iteration algorithm works. Our algorithm has two stages. In the first stage, the iterative point moves in the direction of $\mathbf{c}_u = \sum_{i=1}^{C} a_{u,i}\mathbf{c}_{u,i}$ to the surface of the constraint, where $a_{u,i}$ are given in Appendix **??**. In general, C equals 1 and $\mathbf{c}_u = \mathbf{c}_{u,1}$. From the figure, it is noted that not all points on the surface is the optimal point. The optimal point should be the tangent point between the surface of $J(\mathbf{P}) = J_0$ and the surface of the constraint. In the second stage, the iterative point moves along the surface to approach to the optimal point.

Before the iteration begins, we need to find an initial point of $\mathbf{P}$, such that all $U+2$ constraints are satisfied. The intersection set could be empty if either γ or I_0 is set too high. Such a case indicates the limitations of JCAS waveform designs, i.e., the JCAS waveform sometimes cannot reach the requirements of both radar and communications. Hence, some of the performances for either radar or the communications have to be sacrificed. On the other hand, it should be highlighted that the intersected set of all constraints could be in a very limited space or even a point, given relatively high thresholds of both radar and communications. In this case, by finding the intersection set itself, we can already guarantee the system performance for both radar and communications, and do not need to optimize the metric J. According to Theorem 1, as long as the intersection set is nonempty, we can always maximize J with satisfying all constraints.

Note that we can always let $\mathbf{p}_u = \sum_{i=1}^{N} b_{u,i}\mathbf{q}_i$, where $b_{u,i}$ are arbitrary scaling factors, $\mathbf{q}_i, \forall i \in \{1, \cdots, N\}$, are normalized vectors and satisfy that

$$\begin{aligned} \mathbf{q}_i &= Q_i[(\mathbf{h}_1^{\mathrm{C}}, \cdots, \mathbf{h}_U^{\mathrm{C}}, \mathbf{h}^{\mathrm{S}})^H]^{\dagger}_{:,i}, i \le U+1, \\ \mathbf{q}_j^H \mathbf{q}_i &= 0, U+1 < j \le N, \forall i \in \{1, \cdots, N\}, j \ne i, \end{aligned} \tag{20}$$

where Q_i is a scaling factor, such that $\|\mathbf{q}_i\|_F^2 = 1$. Note that $\mathbf{q}_i, \forall i \in \{1, \cdots, N\}$, form the entire space of N dimension. In the JCAS optimization problem, there are $U+2$ constraints in total. By substituting $\mathbf{p}_u$ into $\|\mathbf{P}\|_F^2 \le U$, we have

$$\sum_{u=1}^{U}\sum_{i=1}^{N} b_{u,i}^2 \le U. \tag{21}$$

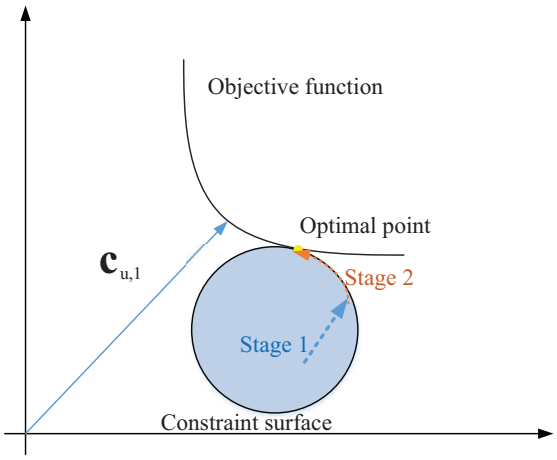

Fig. 2. Explanation of the principle of the proposed iterative Algorithm 1.

By substituting $\mathbf{p}_u$ into the MI constraint, we have

$$\log_2\left(\sigma^{-2}P\sum_{u=1}^{U} b_{u,U+1}^2\|\mathbf{h}^{\mathrm{S}}\|_2^2 + 1\right) \ge I_0. \tag{22}$$

By substituting $\mathbf{p}_u$ into $R_u \ge 0$, we have

$$b_{u,u}^2\|\mathbf{h}_u^{\mathrm{C}}\|_2^2 - \gamma\left(\sum_{v\ne u} b_{v,u}^2\|\mathbf{h}_u^{\mathrm{C}}\|_2^2 + \frac{\sigma_{\mathrm{C}}^2 U}{P}\right) \ge 0. \tag{23}$$

By letting $b_{u,i}^2 = x_{u,i} \ge 0$, all constraints form a convex intersection set, i.e.,

$$\begin{cases} \sum_{u=1}^{U}\sum_{i=1}^{N} x_{u,i} \le U \\ \sum_{u=1}^{U} \|\mathbf{h}^{\mathrm{S}}\|_2^2 x_{u,U+1} \le 2^{I_0}\sigma^2/P - 1 \\ x_{u,u}\|\mathbf{h}_u^{\mathrm{C}}\|_2^2 - \gamma\left(\sum_{v\ne u} x_{v,u}\|\mathbf{h}_u^{\mathrm{C}}\|_2^2\right) \ge \gamma\frac{\sigma_{\mathrm{C}}^2 U}{P} \\ x_{u,i} \ge 0 \end{cases} \tag{24}$$

It is clear that all constraints form a convex set that is intersected by multiple planes in the space of $(x_{1,1}, \cdots, x_{U,N})$. As long as this intersection set is not empty, we can choose $\{b_{u,i}\}s$ that make all constraints be held. Then during iterations, we need all these constraints to be held and make J increase iteratively.

1) **Stage 1:** Now, we give the details of our proposed algorithm. We have obtained a $\mathbf{P}$, such that $\sum_{u=1}^{U}\|\mathbf{p}_u\|_F^2 \le U$ and $\|\mathbf{\Lambda}\|_F^2 \ge \frac{\sigma^2(2^{I_0}-1)}{Ph}$ and $R_u \ge 0$. The current iterative point of $\mathbf{P}$ is denoted as $\mathbf{P}^{(i)}$ and each column of $\mathbf{P}^{(i)}$ is $\mathbf{p}_u^{(i)}$.

We generate two new vectors moving in the directions of $\mathbf{c}_u$.

$$\mathbf{p}_{u-}^{(i)} = \mathbf{p}_u^{(i)} - \epsilon\mathbf{c}_u, \mathbf{p}_{u+}^{(i)} = \mathbf{p}_u^{(i)} + \epsilon\mathbf{c}_u. \tag{25}$$

According to the derivations in Appendix **??**, only one of the two vectors defined in (25) can make the objective function

Algorithm 1 JCAS Precoder Optimization with MI Constraint

Input: $\mathbf{h}^{\mathrm{S}}$ and $\{\mathbf{C}_u\}_{u=1}^{U}$.
Initialization: $i=0$, $J(\mathbf{P}^{(-1)})=-\infty$, I_0,
Obtain $\mathbf{c}_{u,i}$ that is the eigenvector corresponding to the positive eigenvalues.
Find $\mathbf{P}^{(i)}$ satisfying all three constraints.
Stage 1:
while $\sum_{u=1}^{U}\|\mathbf{p}_u\|_F^2 < U$ and$\|\mathbf{\Lambda}\|_F^2 > \frac{\sigma^2(2^{I_0}-1)}{Ph}$ **do**
  Obtain $\mathbf{p}_{u\pm}^{(i)}$ according to (25).
  Obtain next iterative vectors, $\mathbf{p}_u^{(i+1)}$, according to (26).
  $i=i+1$.
end while
Stage 2:
while $J(\mathbf{P}^{(i)}) > J(\mathbf{P}^{(i-1)})$ **do**
  Obtain $\breve{\mathbf{p}}_{u\pm}^{(i)}$ according to (28).
  Obtain next iterative vectors, $\mathbf{p}_u^{(i+1)}$, according to (30).
  $i=i+1$.
end while
Output: $\mathbf{P}$.

increase. We select the one that makes J increase as the next iterative point.

$$\mathbf{p}_u^{(i+1)} = \begin{cases} \mathbf{p}_{u-}^{(i+1)} & \text{if } J(\mathbf{p}_{u-}^{(i+1)}) > J(\mathbf{p}_{u+}^{(i+1)}) \\ \mathbf{p}_{u+}^{(i+1)} & \text{else} \end{cases} \tag{26}$$

2) **Stage 2:** When the iterative point is already on the surface, we generate two precoding vectors moving in the directions of $\mathbf{c}_u$.

$$\mathbf{p}_{u-}^{(i)} = \mathbf{p}_u^{(i)} - \epsilon\mathbf{c}_u, \mathbf{p}_{u+}^{(i)} = \mathbf{p}_u^{(i)} + \epsilon\mathbf{c}_u, \tag{27}$$

where $\mathbf{p}_u^{(i)}$ is on the surface of the constraint, while $\mathbf{p}_{u-}^{(i)}$ and $\mathbf{p}_{u+}^{(i)}$ are not. Since these two vectors are not on the surface of the constraints, we project them onto the surface of the constraint, i.e.,

$$\mathbf{p}_{u-}^{(i)} = \sum_{i=1}^{N} b'_{u,i}\mathbf{q}_i, \mathbf{p}_{u+}^{(i)} = \sum_{i=1}^{N} b''_{u,i}\mathbf{q}_i. \tag{28}$$

It is noted that $b'_{u,i}$, $b''_{u,i}$, and $\mathbf{q}_i$ are known, given $\mathbf{p}_{u-}^{(i)}$ and $\mathbf{p}_{u+}^{(i)}$. If $\mathbf{p}_u^{(i)}$ reaches the surface of $R_u=0$, we only need to adjust $b'_{u,i}$ and $b''_{u,i}$, such that $\mathbf{p}_{u-}^{(i)}$ and $\mathbf{p}_{u+}^{(i)}$ can reach the surface. If $\mathbf{p}_u^{(i)}$ reaches the surface of $\|\mathbf{\Lambda}\|_F^2 = \frac{\sigma^2(2^{I_0}-1)}{Ph}$, we only need to adjust $b'_{U+1,i}$ and $b''_{U+1,i}$, such that the new vectors are projected onto the surface. If $\mathbf{p}_u^{(i)}$ reaches the surface of $\|\mathbf{P}\|_F^2 = U$, we only need to adjust the length of the new vectors, such that they are on the surface. The projected vectors are given by

$$\breve{\mathbf{p}}_{u-}^{(i+1)} = \mathcal{P}\{\mathbf{p}_{u-}^{(i)}\}, \breve{\mathbf{p}}_{u+}^{(i+1)} = \mathcal{P}\{\mathbf{p}_{u+}^{(i)}\}, \tag{29}$$

where $\mathcal{P}$ denotes the projection function. One of the two vectors in (28) should make the objective function keep rising. We select the one that makes J increase as the next iterative point.

$$\mathbf{p}_u^{(i+1)} = \begin{cases} \breve{\mathbf{p}}_{u-}^{(i+1)} & \text{if } J(\breve{\mathbf{p}}_{u-}^{(i+1)}) > J(\breve{\mathbf{p}}_{u+}^{(i+1)}) \\ \breve{\mathbf{p}}_{u+}^{(i+1)} & \text{else} \end{cases}. \tag{30}$$

Update the iteration index $i=i+1$ and repeat the same procedure in Stage 2. We terminate the iteration when $J(\mathbf{p}_u^{(i+1)})$ stop rising.

C. Complexity Analysis

In this subsection, we analyze the computational complexity of Algorithm 1. The main computation tasks in Algorithm 1 include the eigen-decomposition of $\mathbf{C}_u$ and the iterations. The complexity of the eigen-decomposition of $\mathbf{C}_u$ can be given by $\mathcal{O}(N^3)$. Since there are UK $\mathbf{C}_{k,u}$, the total complexity of eigen-decomposition is $\mathcal{O}(N^3UK)$. After obtaining the eigenvectors, the main computational task is the calculation of J_k, which has a complexity of $\mathcal{O}(2N^2U)$ for each J_k in each iteration. The total complexity of obtaining all J_k is $\mathcal{O}(2N^2UKI_i)$ with I_i being the number of iterations. The overall complexity is $\max(\mathcal{O}(N^3UK), \mathcal{O}(2N^2UKI_i))$.

V. CRB Constrained JCAS Waveform Optimization

In this section, we optimize the communication metric by constraining the radar CRB. For individual CRB optimization, we have obtained the covariance matrix of the waveform, i.e., $\mathbf{Q}[k]=\mathbf{P}^H[k]\mathbf{P}[k]$, and the corresponding waveform matrix, $\mathbf{P}_{\mathrm{crb}}[k]$. We constrain the CRB by limiting the Euclidean distance between the optimal CRB and the JCAS waveform matrices. The communication metric is still the proposed J_k. The JCAS optimization problem with the CRB constraint is formulated as

$$\begin{aligned} &\arg\max_{\mathbf{P}[k]} J_k \\ &\text{s.t.}\|\mathbf{P}[k]-\mathbf{P}_{\mathrm{crb}}[k]\|_F^2 \le \xi, \|\mathbf{P}[k]\|_F^2 \le U, R_{k,u} \ge 0, \end{aligned} \tag{31}$$

where ξ is a threshold that controls the Euclidean distance between $\mathbf{P}[k]$ and $\mathbf{P}_{\mathrm{crb}}[k]$. For simplicity of notation, we omit k in the rest of this subsection.

The problem above can be solved in a way similar to the MI constrained problem. The transformed CRB constrained problem can be seen as a quadratic problem with convex constraints. The closed-form solution also exists. Referring to Theorem 1, the closed-form solution can be obtained when $\sum_{i=1}^{C} a_{u,i}\mathbf{c}_{u,i}$ can reach one of the constraint surfaces. When the closed-form solution does not exist, we propose an iteration algorithm.

1) **Stage 1:** We need to obtain a $\mathbf{P}$, such that $\|\mathbf{P}\|_F^2 \le U$, and $\|\mathbf{P}-\mathbf{P}_{\mathrm{crb}}\|_F^2 \le \xi$, and $R_u \ge 0$. The current iterative point of $\mathbf{P}$ is denoted as $\mathbf{P}^{(i)}$ and each column of $\mathbf{P}^{(i)}$ is $\mathbf{p}_u^{(i)}$.

Algorithm 2 JCAS Precoder Optimization with CRB Constraint

Input: $\mathbf{P}_{\text{crb}}$ and $\{\mathbf{C}_u\}_{u=1}^{U}$.
Initialization: $i=0$, $J(\mathbf{P}^{(-1)})=-\infty$, ϵ, ξ,
Obtain $\mathbf{c}_{u,i}$ that is the eigenvector of $\mathbf{C}_u$ corresponding to the positive eigenvalues.
Find $\mathbf{P}^{(i)}$ satisfying all three constraints.
Stage 1:
while $\|\mathbf{P}\|_F^2 < U$ and $\|\mathbf{P}-\mathbf{P}_{\text{crb}}\| < \xi$ **do**
  Obtain $\mathbf{p}_{u\pm}^{(i)}$ according to (32).
  Obtain next iterative vectors, $\mathbf{p}_u^{(i+1)}$, according to (**??**).
  $i=i+1$.
end while
Stage 2:
while $J(\mathbf{P}^{(i)}) > J(\mathbf{P}^{(i-1)})$ **do**
  Obtain $\breve{\mathbf{p}}_{u\pm}^{(i)}$ according to (**??**).
  Obtain next iterative vectors, $\mathbf{p}_u^{(i+1)}$, according to (**??**).
  $i=i+1$.
end while
Output: $\mathbf{P}$.

We generate two new precoding vectors moving in the directions of $\mathbf{c}_u=\sum_{i=1}^{C} a_{u,i}\mathbf{c}_{u,i}$, i.e.,

$$\mathbf{p}_{u-}^{(i)}=\mathbf{p}_u^{(i)}-\epsilon\mathbf{c}_u, \mathbf{p}_{u+}^{(i)}=\mathbf{p}_u^{(i)}+\epsilon\mathbf{c}_u. \tag{32}$$

One of the two vectors defined in (32) should make the objective function rise. We select the one that makes J increase as the next iterative point.

$$\mathbf{p}_u^{(i+1)}=\begin{cases}\mathbf{p}_{u-}^{(i+1)} & \text{if } J(\mathbf{p}_{u-}^{(i+1)})>J(\mathbf{p}_{u+}^{(i+1)})\\ \mathbf{p}_{u+}^{(i+1)} & \text{else}\end{cases} \tag{33}$$

2) **Stage 2:** When the vector reaches the surface of a constraint, we still generate two precoding vectors moving in the directions of $\mathbf{c}_u=\sum_{i=1}^{C} a_{u,i}\mathbf{c}_{u,i}$,

$$\mathbf{p}_{u-}^{(i)}=\mathbf{p}_u^{(i)}-\epsilon\mathbf{c}_u, \mathbf{p}_{u+}^{(i)}=\mathbf{p}_u^{(i)}+\epsilon\mathbf{c}_u. \tag{34}$$

In the CRB constrained problem, if $\mathbf{p}_u^{(i)}$ reaches the constraint of $\|\mathbf{P}\|_F^2\le U$ or $\|\mathbf{P}-\mathbf{P}_{\text{crb}}\|_F^2\le\xi$, we can directly scale those precoding vectors onto the surface of the constraint, i.e.,

$$\breve{\mathbf{p}}_{u-}^{(i)}=\mathbf{p}_{u-}^{(i)}a_-, \breve{\mathbf{p}}_{u+}^{(i)}=\mathbf{p}_{u+}^{(i)}a_+. \tag{35}$$

By adjusting the scaling coefficients, $a_+\approx 1$ and $a_-\approx 1$, we can let the vectors be on the surface of the constraint. If $\mathbf{p}_u^{(i)}$ reaches the constraint of $R_u=0$, we adopt the similar method as the MI constrained JCAS optimization to project the new vectors onto the constraint surface. One of the two vectors in (28) should make the objective function keep rising. We select the one that makes J increase as the next iterative point.

$$\mathbf{p}_u^{(i+1)}=\begin{cases}\breve{\mathbf{p}}_{u-}^{(i+1)} & \text{if } J(\breve{\mathbf{p}}_{u-}^{(i+1)})>J(\breve{\mathbf{p}}_{u+}^{(i+1)})\\ \breve{\mathbf{p}}_{u+}^{(i+1)} & \text{else}\end{cases} \tag{36}$$

Update the iteration index $i=i+1$ and repeat the same procedure in Stage 2. We terminate the iteration when $J(\mathbf{p}_u^{(i+1)})$ stop rising. The proposed CRB constrained optimization scheme is summarized in Algorithm **??**.

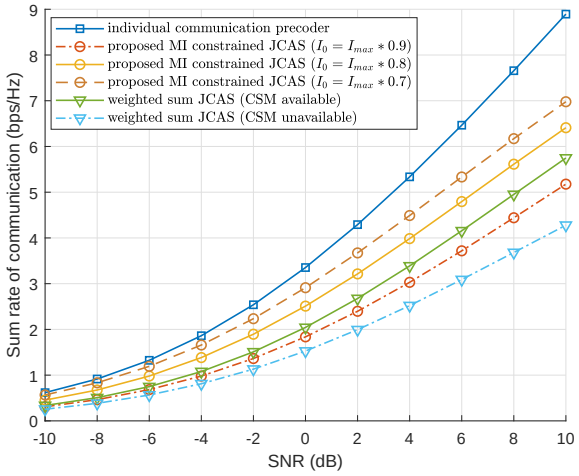

Fig. 3. Sum rate of communications versus SNR with using Algorithm 1 and other bench-marking JCAS solutions.

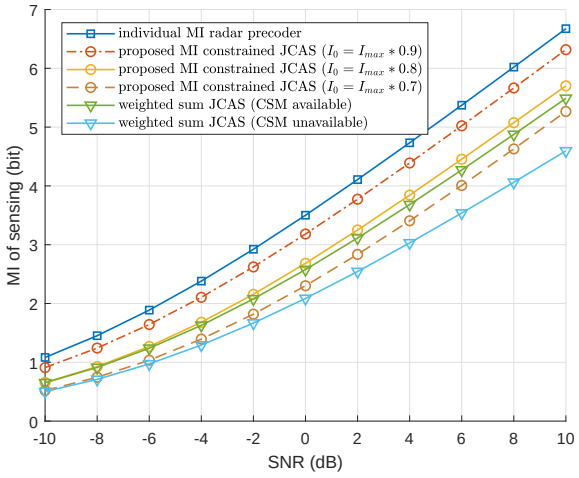

Fig. 4. MI of sensing versus SNR with using Algorithm 1 and other bench-marking JCAS solutions.

VI. Simulation Results

In this section, we provide simulation results to validate the proposed algorithms, using numerical experiments on MATLAB. We simulate a JCAS system where a BS communicates with $U=2$ MUs each having a channel with $L_u=3$ paths, and the BS also needs to sense an environment with $L=3$ targets.

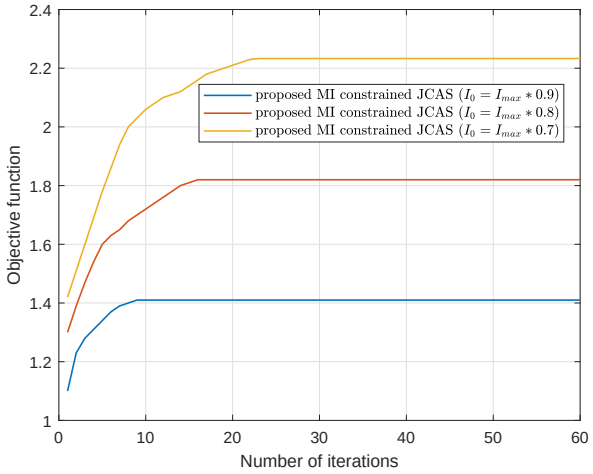

Fig. 5. Objective function of (17) versus the number of iterations.

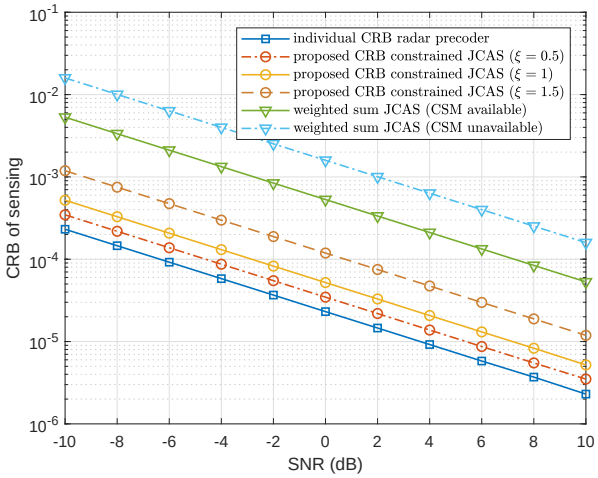

Fig. 7. CRB of sensing versus SNR with using Algorithm 2 and other bench-marking solutions.

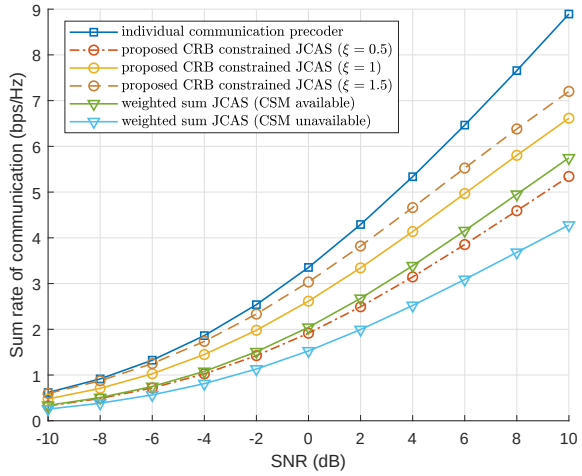

Fig. 6. Sum rate of communications versus SNR with using Algorithm 2 and other bench-marking solutions.

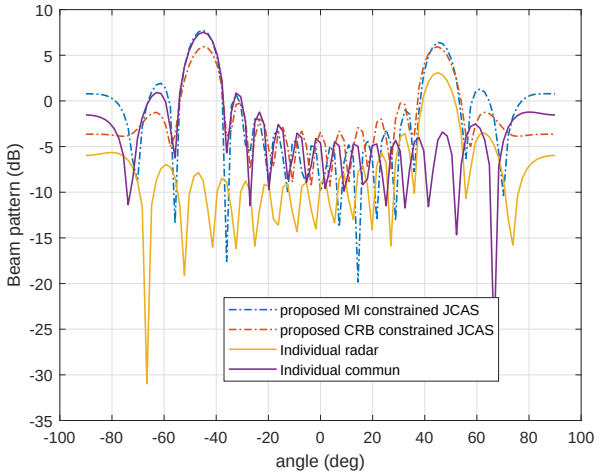

Fig. 8. Beam patterns with employing individual and JCAS solutions.

The BS adopts a 16×1 ULA as the transmit antennas and uses OFDM modulation to transmit a 2×1 data symbol vector on each subcarrier. The number of subcarriers is $K = 512$. The AoDs for both MUs and targets are randomly distributed from $-\pi$ to π. The delay of each path is a random value ranging from 0 to $T/2$. For the parameter in the communication metric, we consider that the data block matrix $\mathbf{S}[k]$ has a dimension of 2×8.

We present the simulation results in three subsections. In the simulation figures, we denote Algorithm 1 as "proposed MI constrained JCAS" and denote Algorithm 2 as "proposed CRB constrained JCAS". In subsection **??**, we show the achieved sum rates for communications, i.e., $\sum_{k=1}^{K}\sum_{u=1}^{U}\log_2(1+\mathrm{SINR}_{k,u})/K/U$, and the achieved MI for radar sensing by using our proposed Algorithm 1. In subsection **??**, we verify the sum rates for communications and the CRB for radar sensing by using our proposed Algorithm 2. In subsection **??**, we compare our proposed algorithms in parallel and intend to find out the connections between using MI and CRB for optimizing JCAS waveforms. For comparison, we compare our proposed algorithms with the bench-marking solutions, including the optimal individual solutions and the weighted sum JCAS solution in [**?**].

A. MI Constrained JCAS

Fig. **??** shows how the sum rates vary with SNR for various waveform optimization schemes. The sum rates of communications rise with SNR increasing. For the individual communication precoder, the sum rate remains the highest, which is as expected because the individual precoder is designed for sum-rate maximization without any radar constraint. For

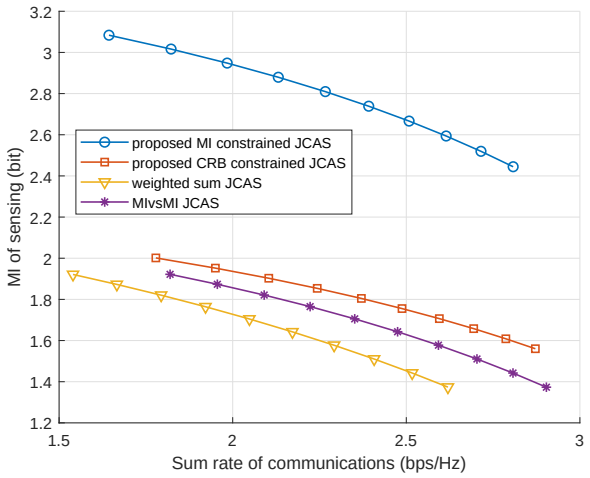

Fig. 9. Sum rate of communications versus MI of sensing.

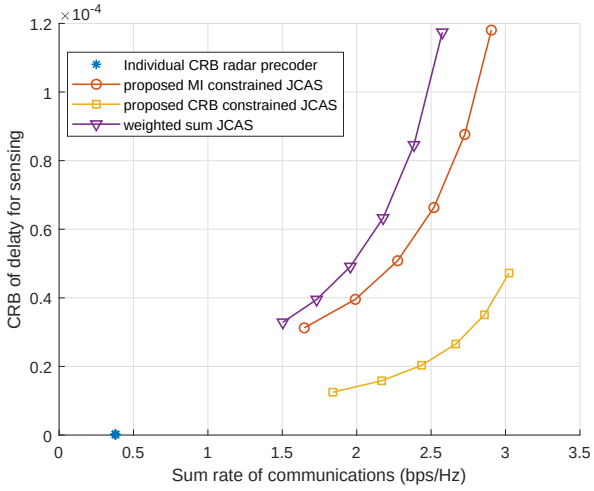

Fig. 10. Sum rate of communications versus CRB of sensing.

JCAS solutions, we compare our proposed Algorithm 1 with the weighted-sum JCAS solution in [**?**]. We define the ratio of I_0 to I_{max} as ρ, where I_{max} is the maximum achievable MI. We see that with ρ ranging from 0.8 to 0.9, our proposed precoder achieves better performance than the weighted-sum JCAS solution. Moreover, the weighted-sum JCAS solution needs a so-called constellation symbol matrix (CSM). When CSM is unavailable, we see that the sum rate of the weighted-sum JCAS solution drops substantially. Comparatively, our proposed algorithm guarantees that the SINR is larger than $\gamma_k = 0.8 \max\left(\sum_{u=1}^{U} \mathrm{SINR}_{k,u}/U\right)$. We can obtain the SINR that is no smaller than γ_k at high SNRs. With the MI threshold I_0 decreasing, we see that the achieved sum rate rises accordingly. This is as expected since our proposed precoder aims to balance between the radar and communication performances. The more demanding the MI requirement of radar is, the smaller the sum rate of communications can be achieved.

Fig. **??** unfolds the achieved MI of radar sensing versus SNR for various waveform optimization schemes. The system setup is the same as that in Fig. **??**. The MI of individual MI radar precoder, i.e., $\mathbf{P}[k] = \mathbf{h}^{\mathrm{S}}[k]\mathbf{\Lambda}[k]$, remains the highest. Our proposed Algorithm 1 achieves higher MI than [**?**] when the MI threshold is no less than $0.8I_{max}$ with I_{max} being the maximum value of MI. Together with Fig. **??**, under the same power control, we observe that the sum rate is inversely proportional to I_0 while the MI is proportional to I_0. To guarantee good performances for both communications and radar sensing, I_0 is around 0.8 I_{max}.

Fig. **??** illustrates how fast the proposed Algorithm 1 can converge. The x-axis is for the number of iterations, i, in Algorithm 1 and the y-axis is for the value of J_k, the objective function in (17). The SNR is fixed at 0 dB. It is noted that the average number of iterations that makes J_k converge is about 10. More iterations lead to higher radar MI. The value of J_k is around 1 to 2 and it rises with decreasing I_0, which indicates that the optimization of J_k with a lower I_0 reaches the surface of the constraints later than that with a higher I_0. The value of J_k determines the gap between the nominator of SINR and the MUI. We note that the value of J_k is smaller than the achieved sum rate and it can be seen as a lower bound of the sum rate.

B. CRB Constrained JCAS

Fig. **??** depicts how the sum rates vary with SNR for the proposed CRB constrained scheme, i.e., Algorithm 2, and other schemes. Similar to Fig. **??**, the sum rate of the individual communication precoder remains the highest. The precoding matrix is normalized to be U. We observe that, overall, our proposed Algorithm 2 achieves better performance than the weighted-sum JCAS solution. With a smaller ξ, the achieved sum rate drops accordingly. The value of ξ represents the Euclidean distance between $\mathbf{P}_{\mathrm{crb}}[k]$ and $\mathbf{P}[k]$. Hence, setting $\xi = 1$ can achieve a balanced performance between radar and communications, as depicted in **??**.

Fig. **??** illustrates the achieved CRB of radar sensing versus SNR. The system setup is the same as that in Fig. **??**. The individual CRB radar precoder achieves the lowest CRB among all schemes. Our proposed Algorithm 2 achieves a low CRB that approaches to the one for the individual optimal scheme. Compared with the method in [**?**], our scheme achieves better performances. By further decreasing ξ to zero, our proposed scheme can achieve the lowest CRB. Together with Fig. **??**, we can set ξ to be around 1 to guarantee good performances for both communication and sensing.

Fig. **??** illustrates an example of JCAS beam patterns employing the proposed algorithms. To make the beam patterns clear to see, we only consider one MU and one target with only one path, i.e., $U = 1$, $L = 1$, and $L_u = 1$. For individual designs as illustrated in section III, we adopt the individual optimal MI radar precoder and the individual optimal communication precoder, respectively. We see that there is only one

main lobe located at around 40° for the radar precoder and only one main lobe located at around -50° for the communication precoder. For JCAS designs, both of our proposed algorithms have two main lobes, matching with the locations of individual designs tightly. At the sidelobes, we see that our proposed JCAS solutions have a larger sidelobe, since our proposed JCAS solutions simultaneously generate two main lobes while the individual designs only need to generate one main lobe.

C. Comparisons of Proposed MI/CRB Constrained JCAS

Fig. **??** plots the sum rate versus the achieved MI of the proposed Algorithm 1 (MI constrained JCAS), Algorithm 2 (CRB constrained JCAS), and other two bench-marking solutions. The system setup is the same as that in Fig. **??**. The x-axis is the sum rate of communications and the y-axis is the achieved MI of radar. For Algorithm 1, we vary the thresholds ρ from 0.7 to 0.9. For Algorithm 2, we vary the threshold ξ from 0.5 to 1.5. For weighted sum JCAS [**?**] that uses a weighting coefficient, μ, we vary μ from 0.4 to 0.6. We name the work in [**?**] as MI-vs-MI JCAS that derived the optimal radar MI waveform and the optimal communication MI waveform in a single-user case. For MI-vs-MI JCAS, we also use μ to balance between the optimal MI waveforms of radar and that of communications. We see that the MI achieved by Algorithm 1 is significantly higher than all other schemes. With the same communication performances, the MI of Algorithm 1 exceeds that of Algorithm 2 by almost 1 bit. This could be explained by noting that the individual CRB radar precoder is close to the array response matrix $\mathbf{A}$ instead of $\mathbf{h}^{\mathrm{S}}[k]\mathbf{\Lambda}[\mathbf{k}]$, which means that some vectors in $\mathbf{A}$ could be truncated when using the CRB precoder, resulting in the decrease of MI. We note that if the curve is convex and approaches to the top-right corner, the curve can be seen as an ideal curve that can satisfy both the sum rates for communications and the MI for radar. Our goal should be to make the curve approach to the top-right corner as much as possible.

Fig. **??** plots the sum rate versus the achieved CRB of the proposed Algorithm 1 (MI constrained JCAS), Algorithm 2 (CRB constrained JCAS), and other bench-marking solutions. The x-axis is the sum rate of communications and the y-axis is the achieved CRB of radar. The ranges of thresholds are the same as those in Fig. **??**. The system setup is the same as that in Fig. **??**. From the figure, we see that the CRB of Algorithm 1 is higher than that of Algorithm 2. This could be explained by the fact that the proposed optimal MI radar precoder only has a rank of 1. Hence, the eigenvalues of FIMs are relatively smaller and result in the increase of CRB. The Algorithm 2's CRB is closed to that of the individual CRB radar precoder, the corresponding achieved sum rate is significantly higher than that of individual radar precoder. The optimal curve should approach to the bottom-right corner that achieves relatively better JCAS performance. Comparing to Fig. **??**, we see that the proposed Algorithm 1 has advantages in MI-based optimizations while the proposed Algorithm 2 has advantages in CRB based optimizations.

VII. Conclusion

In this paper, we have proposed the JCAS precoding optimization algorithms that maximize the developed relaxed SINR under the constraint of either MI or CRB of radar. The adopted radar metrics correspond to two types of individual optimal radar waveforms and the adopted communication precoding vectors maximize the relaxed SINR. The developed relaxed SINR of communication has a quadratic form and can serve as a lower bound for SINR. When the radar targets and the communication users are close to each other, we can obtain the closed-form solution. Otherwise, in more general cases, we can use the proposed iteration algorithms to optimize the JCAS precoders. The simulations provide the valid range of the thresholds and validate the effectiveness of the proposed algorithms. The simulations also show that the proposed MI/CRB constrained JCAS algorithms have their own advantages.

Appendix A
Proof for equality between (8) and (9)

Let $\mathbf{H} \triangleq \mathbf{h}\mathbf{h}^H$ and $\mathbf{Q} \triangleq \mathbf{p}\mathbf{p}^H$. To show that (8) is equal to (9), we only need to prove that $\mathrm{Tr}(\mathbf{QH}) = \mathbf{p}^H\mathbf{H}\mathbf{p}$. We have

$$\mathrm{Tr}(\mathbf{p}\mathbf{p}^H\mathbf{H}) = \mathrm{Tr}(\mathbf{p}^H\mathbf{H}\mathbf{p}) = (\mathbf{p}^H\mathbf{H}\mathbf{p}). \tag{37}$$

Therefore, (8) is equal to (9).

Appendix B
Expression for FIM Subblocks

Referring to the derivation in [**?**], the FIM subblocks are expressed as

$$\begin{aligned}
\mathbf{F}_1 &= \frac{2}{\sigma}\sum_{k=1}^{K}\mathbf{\Phi}^H[k]\mathbf{A}^H\mathbf{P}[k]\mathbf{P}^H[k]\mathbf{A}\mathbf{\Phi}[k]\\
\mathbf{F}_2 &= \frac{2}{\sigma}\sum_{k=1}^{K}\mathbf{\Phi}^H[k]\left(\mathbf{A}^H\mathbf{P}[k]\mathbf{P}^H[k]\mathbf{A}\right)\odot\mathbf{\Psi}\dot{\mathbf{\Phi}}[k]\\
\mathbf{F}_3 &= \frac{2}{\sigma}\sum_{k=1}^{K}\mathbf{\Phi}^H[k]\left(\mathbf{A}^H\mathbf{P}[k]\mathbf{P}^H[k]\dot{\mathbf{A}}\right)\odot\mathbf{\Psi}\mathbf{\Phi}[k]\\
\mathbf{F}_4 &= \frac{2}{\sigma}\sum_{k=1}^{K}\dot{\mathbf{\Phi}}^H[k]\left(\mathbf{A}^H\mathbf{P}[k]\mathbf{P}^H[k]\mathbf{A}\right)\odot(\mathbf{\Psi}^H\mathbf{1}\mathbf{1}^H\mathbf{\Psi})\dot{\mathbf{\Phi}}[k]\\
\mathbf{F}_5 &= \frac{2}{\sigma}\sum_{k=1}^{K}\dot{\mathbf{\Phi}}^H[k]\left(\mathbf{A}^H\mathbf{P}[k]\mathbf{P}^H[k]\dot{\mathbf{A}}\right)\odot(\mathbf{\Psi}^H\mathbf{1}\mathbf{1}^H\mathbf{\Psi})\mathbf{\Phi}[k]\\
\mathbf{F}_6 &= \frac{2}{\sigma}\sum_{k=1}^{K}\mathbf{\Phi}^H[k]\left(\dot{\mathbf{A}}^H\mathbf{P}[k]\mathbf{P}^H[k]\dot{\mathbf{A}}\right)\odot(\mathbf{\Psi}^H\mathbf{1}\mathbf{1}^H\mathbf{\Psi})\mathbf{\Phi}[k],
\end{aligned} \tag{38}$$

where $\odot$ is the Hadamard product,

$$\dot{\mathbf{\Phi}}[k] = \left[\frac{\partial[\mathbf{\Phi}[k]]_{:,1}}{\partial(\tau_1/T)},\cdots,\frac{\partial[\mathbf{\Phi}[k]]_{:,L}}{\partial(\tau_1/T)}\right]$$

$$= -j2\pi k\mathbf{\Phi}[k], \tag{39}$$

and

$$\dot{\mathbf{A}} = \left[\frac{\partial[\mathbf{A}]_{:,1}}{\partial\Omega_1}, \cdots, \frac{\partial[\mathbf{A}]_{:,L}}{\partial\Omega_L}\right]. \tag{40}$$

Appendix C
Proof for the existence of $\bar{\mathbf{P}}[k]$ satisfying $\bar{\mathbf{P}}[k]\bar{\mathbf{P}}^H[k] = \mathbf{Q}[k]$

When there is only one parameter, the expression of $\mathbf{F}$ can be simplified greatly. Following the derivation in [**?**], the FIM of delay is $\mathrm{Re}[\mathbf{F}_4]$, the FIM of angles is $\mathrm{Re}[\mathbf{F}_6]$, and the FIM of the complex path gains is $\mathbf{F}_1$.

When we consider the FIM for only one parameter, we can prove that there is an optimal $\mathbf{P}[k]$ that is not affected by the rank issue of $\mathbf{Q}[k]$. We use $\mathrm{Re}[\mathbf{F}_4]$ as an example to demonstrate the existence of $\mathbf{P}[k]$. For other FIMs in the diagonal entries of $\mathbf{F}$, they hold the same property and can be proven in the same way.

When $\mathbf{F} = \mathrm{Re}[\mathbf{F}_4]$, it is noted that $\mathbf{A}^H\mathbf{Q}[k]\mathbf{A}$ is a low rank matrix with rank being L. The null-space of $\mathbf{A}$ is given by $\mathbf{N}_\mathrm{A}$ and the total space is given by $\mathbf{B} = [\mathbf{A}\,\mathbf{N}_\mathrm{A}]$. Notice that $\mathbf{Q}[k] = \mathbf{B}\mathbf{B}^{-1}\mathbf{Q}[k]\mathbf{B}^{-1}\mathbf{B}$. Let $\bar{\mathbf{B}}[k] \triangleq \mathbf{B}^{-1}\mathbf{Q}[k]\mathbf{B}$. Then, we have

$$\begin{aligned}&\mathbf{A}^H\mathbf{Q}[k]\mathbf{A}\\ =&\mathbf{A}^H\mathbf{B}\mathbf{B}^{-1}\mathbf{Q}[k]\mathbf{B}^{-1}\mathbf{B}\mathbf{A}\\ =&\mathbf{A}^H[\mathbf{A}\,\mathbf{0}]\begin{bmatrix}[\bar{\mathbf{B}}[k]]_{1:L,1:L} & \mathbf{0}\\ \mathbf{0} & \mathbf{0}\end{bmatrix}[\mathbf{A}\,\mathbf{0}]\mathbf{A}.\end{aligned} \tag{41}$$

Now, we can obtain $\mathbf{P}[k] = \mathbf{A}[\bar{\mathbf{B}}[k]]^{\frac{1}{2}}_{1:L,1:L}$. Therefore, we can obtain $\mathbf{P}[k]$ perfectly, such that $\mathbf{P}[k]\mathbf{P}^H[k] = \mathbf{Q}[k]$.

Appendix D
Proof for Lemma 1

We write J as

$$J = \sum_{u=1}^{U}\mathbf{p}_u^H\mathbf{C}_u\mathbf{p}_u. \tag{42}$$

Next, we prove that any point of $\mathbf{p}_u$ cannot maximize J when there is no constraint, which equivalently means that the optimal value is achieved on the constraint surface.

We express $\mathbf{p}_u$ as $\mathbf{v}_u + \mathbf{w}_u$, where $\mathbf{v}_u$ is given by $\frac{\mathbf{h}^\mathrm{S}(\mathbf{h}^\mathrm{S})^H\mathbf{p}_u}{\|\mathbf{h}^\mathrm{S}\|_F^2}$, and $\mathbf{w}_u$ is given by $\mathbf{p}_u - \mathbf{v}_u$. For any given point of $\{\mathbf{p}'_u\}_{u=1}^U$ that is inside the surfaces of all three constraints, we can find a new vector, $\mathbf{p}''_u = \mathbf{p}'_u + \epsilon\mathbf{c}_{u,i}$, where $\mathbf{c}_{u,i}$ is the ith eigenvector of $\mathbf{C}_u$ corresponding to the positive eigenvalue. The variable, $\epsilon > 0$, is small enough to make the new vector still be inside the surfaces of the constraints. Then, the new vector satisfies

$$\begin{aligned}J(\mathbf{p}''_u) =&J(\mathbf{p}'_u + \epsilon\mathbf{c}_{u,i})\\ =&J(\mathbf{p}'_u) + 2\epsilon r_{u,i}\bar{\mathbf{c}}_{u,i}^T\bar{\mathbf{p}}'_u + \epsilon^2 r_{u,i},\end{aligned} \tag{43}$$

where $\bar{\mathbf{c}}_{u,i} = \left[\mathrm{Re}[\mathbf{c}_{u,i}]^T, \mathrm{Im}[\mathbf{c}_{u,i}]^T\right]^T$ and $\bar{\mathbf{p}}_u = \left[\mathrm{Re}[\mathbf{p}_u]^T, \mathrm{Im}[\mathbf{p}_u]^T\right]^T$. It is clear that the third term of (**??**) is positive. If the second term is also positive, we have $J(\mathbf{p}''_u) > J(\mathbf{p}'_u)$. Hence, J keeps rising until the vector reaches one out of the three constraint surfaces. If the second term in (**??**) is negative, then we choose the opposite vector, i.e., $\mathbf{p}''_u = \mathbf{p}'_u - \epsilon\mathbf{c}_{u,1}$, and the second term becomes positive. Therefore, the optimal value of $\mathbf{p}_u$ is on one of the constraint surfaces.

Appendix E
Proof for Theorem 1

For a given vector, $\mathbf{p}_u$, it can be expressed as a linear function of all eigenvectors of $\mathbf{C}_u$, i.e., $\mathbf{p}_u = \sum_{i=1}^{N}\mathbf{c}_{u,i}a_{u,i}$, where $\mathbf{c}_{u,i}$ is the ith eigenvector of $\mathbf{C}_u$ and $a_{u,i}$ is a weighting coefficient. The rank of $\mathbf{C}_u$ is L and the number of positive eigenvalues of $\mathbf{C}_u$ is C. Then we have

$$J(\mathbf{p}_u) = \sum_{u=1}^{U}\sum_{i=1}^{N} r_{u,i}a_{u,i}^2, \tag{44}$$

where $r_{u,i}$ is the ith eigenvalue of $\mathbf{C}_u$. According to Lemma 1, the optimal point must be on the surface of the constraints, which means that one out of three equality constraints is satisfied.

When the constraint of $\|\mathbf{P}\|_F^2 = U$ is satisfied, the weighting coefficients satisfy that $\sum_{u=1}^{U}\sum_{i=1}^{N} a_{u,i}^2 = U$. Then we can obtain the optimal values for $a_{u,i}$, i.e.,

$$a_{u,i}^2 = \begin{cases}\frac{r_{u,i}}{D}, & i = 1\\ 0, & else\end{cases}, \tag{45}$$

where D is a factor, such that $\sum_{u=1}^{U}\sum_{i=1}^{N} a_{u,i}^2 = U$.

When $\mathbf{p}_u$ reaches the surface of $\|\mathbf{\Lambda}\|_F^2 = \frac{\sigma^2(2^{I_0}-1)}{Ph}$, the weighting coefficients satisfy

$$\sum_{u=1}^{U}\left|\sum_{i=1}^{N}(\mathbf{h}^\mathrm{S})^H\mathbf{c}_{u,i}a_{u,i}\right|^2 = \frac{\sigma^2(2^{I_0}-1)}{P}. \tag{46}$$

We note that the phase of $a_{u,i}$ has no impacts on J, which means that we can let the phase of $a_{u,i}$ be $e^{j\angle\mathbf{c}_{u,i}^H\mathbf{h}^\mathrm{S}}$. Then, we have

$$\sum_{u=1}^{U}\left|\sum_{i=1}^{N}\left|(\mathbf{h}^\mathrm{S})^H\mathbf{c}_{u,i}\right||a_{u,i}|\right|^2 = \frac{\sigma^2(2^{I_0}-1)}{P}. \tag{47}$$

Note that this is a convex optimization problem, we can solve the modulus of $a_{u,i}$ using convex optimization toolboxes. Hence, the optimal values for $a_{u,i}$ are

$$a_{u,i} = \begin{cases}|a_{u,i}|^\star e^{j\angle\mathbf{c}_{u,i}^H\mathbf{h}^\mathrm{S}}, & i \le C\\ 0, & else\end{cases}. \tag{48}$$

Under the constraint of $\mathbf{p}_u^H \mathbf{H}_u \mathbf{p}_u - \gamma \sum_{v \neq u} \mathbf{p}_v^H \mathbf{H}_u \mathbf{p}_v = \gamma \frac{\sigma_C^2 U}{P}$, we optimize $J = \sum_{u=1}^{U} \mathbf{p}_u^H \mathbf{C}_u \mathbf{p}_u$. Substituting the constraint into the objective function, we have $J = \gamma \frac{\sigma_C^2 U}{P} + \sum_{v \neq u} \mathbf{p}_v^H \mathbf{H}_v \mathbf{p}_v - \gamma \sum_{u \neq v} \mathbf{p}_u^H \mathbf{H}_v \mathbf{p}_u = \frac{\sigma_C^2 U}{P} + \sum_{v \neq u} R_{k,v} \geq \gamma \frac{\sigma_C^2 U^2}{P}$. Note that the thresholds γ is the same for all users, which means that we can only let the user with the smallest optimal $R_{k,u}$ meet this constraint. Hence, in this case, the closed-form solution is the same as the conventional communication solution in (11).

Appendix F
Proof for Corollary 1

According to Lemma 1, the optimal point of $\mathbf{P}$ is on the surface of constraints. For simplicity, we assume that the optimal $\mathbf{P}$ is achieved when $\|\mathbf{P}\|_F^2 = U$. In this case, the surface of $J(\mathbf{P}) = J_0$ and the surface of $\|\mathbf{P}\|_F^2 = U$ are tangent with each other. Otherwise, there will be a point of $\mathbf{P}$ that satisfies $J(\mathbf{P}) = J_0$ and $\|\mathbf{P}\|_F^2 < U$, which is contradictory with Theorem 1. Therefore, the optimal point of $\mathbf{P}$ is on the tangent plane of $J(\mathbf{P}) = J_0$.

References

[1] A. Abdelhadi and T. C. Clancy, "Network MIMO with partial cooperation between radar and cellular systems," in *2016 International Conference on Computing, Networking and Communications (ICNC)*, Feb. 2016, pp. 1–5.

[2] M. L. Rahman, J. A. Zhang, X. Huang, Y. J. Guo, and R. W. Heath, "Framework for a perceptive mobile network using joint communication and radar sensing," *IEEE Trans. Aerosp. Electron. Syst.*, vol. 56, no. 3, pp. 1926–1941, Jun. 2020.

[3] J. A. Zhang, M. L. Rahman, K. Wu, X. Huang, Y. J. Guo, S. Chen, and J. Yuan, "Enabling joint communication and radar sensing in mobile networks-a survey," *IEEE Communications Surveys & Tutorials*, 2021.

[4] F. Liu, C. Masouros, A. P. Petropulu, H. Griffiths, and L. Hanzo, "Joint radar and communication design: Applications, state-of-the-art, and the road ahead," *IEEE Trans. Commun.*, vol. 68, no. 6, pp. 3834–3862, Jun. 2020.

[5] P. Kumari, J. Choi, N. González-Prelcic, and R. W. Heath, "IEEE 802.11ad-based radar: An approach to joint vehicular communication-radar system," *IEEE Trans. Veh. Technol.*, vol. 67, no. 4, pp. 3012–3027, Apr. 2018.

[6] R. C. Daniels, E. R. Yeh, and R. W. Heath, "Forward collision vehicular radar with IEEE 802.11: Feasibility demonstration through measurements," *IEEE Trans. Veh. Technol.*, vol. 67, no. 2, pp. 1404–1416, Feb. 2018.

[7] S. H. Dokhanchi, M. R. B. Shankar, Y. A. Nijsure, T. Stifter, S. Sedighi, and B. Ottersten, "Joint automotive radar-communications waveform design," in *2017 IEEE 28th Annual International Symposium on Personal, Indoor, and Mobile Radio Communications (PIMRC)*, 2017, pp. 1–7.

[8] X. Li, D. Zhang, Q. Lv, J. Xiong, S. Li, Y. Zhang, and H. Mei, "Indotrack: Device-free indoor human tracking with commodity Wi-Fi," *Proc. ACM Interact. Mob. Wearable Ubiquitous Technol.*, vol. 1, no. 3, Sep. 2017. [Online]. Available: https://doi.org/10.1145/3130940

[9] K. Qian, C. Wu, Y. Zhang, G. Zhang, Z. Yang, and Y. Liu, "Widar2.0: Passive human tracking with a single Wi-Fi link," in *Proceedings of the 16th Annual International Conference on Mobile Systems, Applications, and Services*. New York, NY, USA: Association for Computing Machinery, 2018, pp. 350–361. [Online]. Available: https://doi.org/10.1145/3210240.3210314

[10] D. Garmatyuk, P. Giza, N. Condict, and S. Mudaliar, "Randomized OFDM waveforms for simultaneous radar operation and asynchronous covert communications," in *2018 IEEE Radar Conference (RadarConf18)*, 2018, pp. 0975–0980.

[11] C. Sturm and W. Wiesbeck, "Waveform design and signal processing aspects for fusion of wireless communications and radar sensing," *Proc. IEEE*, vol. 99, no. 7, pp. 1236–1259, Jul. 2011.

[12] A. R. Chiriyath, B. Paul, and D. W. Bliss, "Radar-communications convergence: Coexistence, cooperation, and co-design," *IEEE Trans. on Cogn. Commun. Netw.*, vol. 3, no. 1, pp. 1–12, Mar. 2017.

[13] L. Han and K. Wu, "Joint wireless communication and radar sensing systems - state of the art and future prospects," *IET Microwaves, Antennas Propagation*, vol. 7, no. 11, pp. 876–885, Aug. 2013.

[14] Y. Liu, G. Liao, Z. Yang, and J. Xu, "Multiobjective optimal waveform design for OFDM integrated radar and communication systems," *Signal Process.*, vol. 141, pp. 331–342, Jun. 2017.

[15] A. Hassanien, M. G. Amin, E. Aboutanios, and B. Himed, "Dual-function radar communication systems: A solution to the spectrum congestion problem," *IEEE Signal Process. Mag.*, vol. 36, no. 5, pp. 115–126, Sep. 2019.

[16] A. Hassanien, M. G. Amin, Y. D. Zhang, and F. Ahmad, "Dual-function radar-communications: Information embedding using sidelobe control and waveform diversity," *IEEE Trans. Signal Process.*, vol. 64, no. 8, pp. 2168–2181, Apr. 2016.

[17] J. Qian, M. Lops, L. Zheng, X. Wang, and Z. He, "Joint system design for coexistence of MIMO radar and MIMO communication," *IEEE Trans. Signal Process.*, vol. 66, no. 13, pp. 3504–3519, Jul. 2018.

[18] Y. L. Sit and T. Zwick, "MIMO OFDM radar with communication and interference cancellation features," in *2014 IEEE radar conference*, 2014, pp. 0265–0268.

[19] J. A. Zhang, X. Huang, Y. J. Guo, J. Yuan, and R. W. Heath, "Multibeam for joint communication and radar sensing using steerable analog antenna arrays," *IEEE Trans. Veh. Technol.*, vol. 68, no. 1, pp. 671–685, Jan. 2019.

[20] Y. Luo, J. A. Zhang, X. Huang, W. Ni, and J. Pan, "Optimization and quantization of multibeam beamforming vector for joint communication and radio sensing," *IEEE Trans. Commun.*, vol. 67, no. 9, pp. 6468–6482, Sep. 2019.

[21] F. Liu, C. Masouros, A. Li, H. Sun, and L. Hanzo, "MU-MIMO communications with MIMO radar: From co-existence to joint transmission," *IEEE Trans. Wireless Commun.*, vol. 17, no. 4, pp. 2755–2770, Apr. 2018.

[22] F. Liu, L. Zhou, C. Masouros, A. Li, W. Luo, and A. Petropulu, "Toward dual-functional radar-communication systems: Optimal waveform design," *IEEE Trans. Signal Process.*, vol. 66, no. 16, pp. 4264–4279, Aug. 2018.

[23] B. Li and A. Petropulu, "MIMO radar and communication spectrum sharing with clutter mitigation," in *2016 IEEE Radar Conference (RadarConf)*, May 2016, pp. 1–6.

[24] B. Li, A. P. Petropulu, and W. Trappe, "Optimum co-design for spectrum sharing between matrix completion based MIMO radars and a MIMO communication system," *IEEE Trans. Signal Process.*, vol. 64, no. 17, pp. 4562–4575, Sep. 2016.

[25] B. Li and A. P. Petropulu, "Joint transmit designs for coexistence of MIMO wireless communications and sparse sensing radars in clutter," *IEEE Trans. Aerosp. Electron. Syst.*, vol. 53, no. 6, pp. 2846–2864, Dec. 2017.

[26] Y. L. Sit, B. Nuss, and T. Zwick, "On mutual interference cancellation in a MIMO OFDM multiuser radar-communication network," *IEEE Trans. Veh. Technol.*, vol. 67, no. 4, pp. 3339–3348, Apr. 2018.

[27] Z. Ni, A. Zhang, K. Yang, F. Gao, and J. An, "Hybrid precoder design with minimum-subspace-distortion quantization in multiuser mmwave communications," *IEEE Trans. Veh. Technol.*, pp. 1–1, 2020.

[28] C. Sturm, Y. L. Sit, M. Braun, and T. Zwick, "Spectrally interleaved multi-carrier signals for radar network applications and multi-input multi-output radar," *IET Radar, Sonar Navigation*, vol. 7, no. 3, pp. 261–269, Mar. 2013.

[29] Y. Liu, G. Liao, J. Xu, Z. Yang, and Y. Zhang, "Adaptive OFDM integrated radar and communications waveform design based on information theory," *IEEE Commun. Lett.*, vol. 21, no. 10, pp. 2174–2177, Oct. 2017.

[30] A. Turlapaty and Y. Jin, "A joint design of transmit waveforms for radar and communications systems in coexistence," in *2014 IEEE Radar Conference*, 2014, pp. 0315–0319.

[31] A. R. Chiriyath, B. Paul, G. M. Jacyna, and D. W. Bliss, "Inner bounds on performance of radar and communications co-existence," *IEEE Trans. Signal Process.*, vol. 64, no. 2, pp. 464–474, 2015.

[32] B. Paul and D. W. Bliss, "Estimation information bounds using the I-MMSE formula and gaussian mixture models," in *2016 Annual Conference on Information Science and Systems (CISS)*, 2016, pp. 274–279.

[33] Z. Zhang, X. Chai, K. Long, A. V. Vasilakos, and L. Hanzo, "Full duplex techniques for 5G networks: self-interference cancellation, protocol design, and relay selection," *IEEE Commun. Mag.*, vol. 53, no. 5, pp. 128–137, May 2015.

[34] Z. Ni, J. A. Zhang, X. Huang, K. Yang, and F. Gao, "Parameter estimation and signal optimization for joint communication and radar sensing," in *2020 IEEE International Conference on Communications Workshops (ICC Workshops)*, 2020, pp. 1–6.

[35] A. Melzer, A. Onic, F. Starzer, and M. Huemer, "Short-range leakage cancelation in FMCW radar transceivers using an artificial on-chip target," *IEEE J. Sel. Topics Signal Process.*, vol. 9, no. 8, pp. 1650–1660, Dec. 2015.

[36] K. Lin, Y. E. Wang, C.-K. Pao, and Y.-C. Shih, "A *ka*-band FMCW radar front-end with adaptive leakage cancellation," *IEEE Trans. Microw. Theory Tech.*, vol. 54, no. 12, pp. 4041–4048, Dec. 2006.

[37] P. Almers, E. Bonek, A. Burr, N. Czink, M. Debbah, V. Degli-Esposti, H. Hofstetter, P. Kyösti, D. Laurenson, G. Matz *et al.*, "Survey of channel and radio propagation models for wireless MIMO systems," *EURASIP Journal on Wireless Communications and Networking*, vol. 2007, pp. 1–19, 2007.

[38] Z.-q. Luo, W.-k. Ma, A. M.-c. So, Y. Ye, and S. Zhang, "Semidefinite relaxation of quadratic optimization problems," *IEEE Signal Process. Mag.*, vol. 27, no. 3, pp. 20–34, Apr. 2010.

[39] Y. Huang and D. P. Palomar, "Rank-constrained separable semidefinite programming with applications to optimal beamforming," *IEEE Trans. Signal Process.*, vol. 58, no. 2, pp. 664–678, Feb. 2010.

[40] R. Xu, L. Peng, W. Zhao, and Z. Mi, "Radar mutual information and communication channel capacity of integrated radar-communication system using MIMO," *ICT Express*, vol. 1, no. 3, pp. 102–105, Jan. 2016.

[41] M. D. Larsen, A. L. Swindlehurst, and T. Svantesson, "Performance bounds for MIMO-OFDM channel estimation," *IEEE Trans. Signal Process.*, vol. 57, no. 5, pp. 1901–1916, May 2009.

[42] L. Xu, J. Li, P. Stoica, K. W. Forsythe, and D. W. Bliss, "Waveform optimization for MIMO radar: A Cramér-Rao bound based study," in *2007 IEEE International Conference on Acoustics, Speech and Signal Processing - ICASSP '07*, vol. 2, 2007, pp. II–917–II–920.

[43] J. J. Moré and D. C. Sorensen, "Newton's method," Argonne National Lab., IL (USA), Tech. Rep., 1982.

Zhitong Ni received the B.E. degree in information engineering from Beijing Institute of Technology, Beijing, China, in 2017. He is currently pursuing the Ph.D. degree with Beijing Institute of Technology, China, and University of Technology Sydney, Australia. His research interests include array signal processing, angle-of-arrival estimations, as well as precoding techniques in various applications including the fifth-generation millimeter-wave communications and joint radar and communication (Rad-Com) systems.

J. Andrew Zhang (M'04-SM'11) received B.Sc. degree from Xi'an JiaoTong University, China, in 1996, M.Sc. degree from Nanjing University of Posts and Telecommunications, China, in 1999, and Ph.D. degree from the Australian National University, in 2004. Currently, He is an Associate Professor in the School of Electrical and Data Engineering and the director of the Radio Sensing and Pattern Analysis (RaSPA) laboratory, University of Technology Sydney, Australia. He was a researcher with Data61, CSIRO, Australia from 2010 to 2016, the Networked Systems, NICTA, Australia from 2004 to 2010, and ZTE Corp., Nanjing, China from 1999 to 2001.

Dr. Zhang's research interests are in the area of signal processing for wireless communications and sensing, with current focuses on joint communications and radio/radar sensing, and autonomous vehicular networks. He has published over 200 journal and conference papers, and has won 5 best paper awards including in IEEE ICC 2013. He is a recipient of CSIRO Chairman's Medal and the Australian Engineering Innovation Award in 2012 for exceptional research achievements in multi-gigabit wireless communications.

Kai Yang (M'12) received the B.E. and Ph.D. degrees from National University of Defense Technology and Beijing Institute of Technology, China, in 2005 and 2010, respectively, both in communications engineering. From Jan. 2010 to July 2010, he was with the Department of Electronic and Information Engineering, Hong Kong Polytechnic University. From 2010 to 2013, he was with Alcatel-Lucent Shanghai Bell, Shanghai, China. In 2013, he joined the Laboratoire de Recherche en Informatique, University Paris Sud 11, Orsay, France. Now, he is with the School of Information and Electronics, Beijing Institute of Technology, Beijing, China. His current research interests include convex optimization, massive MIMO, mmWave systems, resource allocation, and interference mitigation.

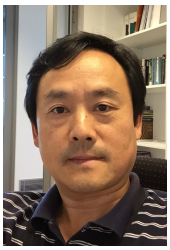

Xiaojing Huang (M'99-SM'11) received the B.Eng., M.Eng., and Ph.D. degrees in electronic engineering from Shanghai Jiao Tong University, Shanghai, China, in 1983, 1986, and 1989, respectively. He was a Principal Research Engineer with the Motorola Australian Research Center, Botany, NSW, Australia, from 1998 to 2003, and an Associate Professor with the University of Wollongong, Wollongong, NSW, Australia, from 2004 to 2008. He had been a Principal Research Scientist with the Commonwealth Scientific and Industrial Research Organisation (CSIRO), Sydney, NSW, Australia, and the Project Leader of the CSIRO Microwave and mmWave Backhaul projects since 2009. He is currently a Professor of Information and Communications Technology with the School of Electrical and Data Engineering and the Program Leader for Mobile Sensing and Communications with the Global Big Data Technologies Center, University of Technology Sydney (UTS), Sydney, NSW, Australia. His research interests include high-speed wireless communications, digital and analog signal processing, and synthetic aperture radar imaging. With over 32 years of combined industrial, academic, and scientific research experience, he has authored over 330 book chapters, refereed journal and conference papers, major commercial research reports, and filed 31 patents. Prof. Huang was a recipient of the CSIRO Chairman's Medal and the Australian Engineering Innovation Award in 2012 for exceptional research achievements in multigigabit wireless communications.

Theodoros A. Tsiftsis (S'02, M'04, SM'10) received the PhD degree in electrical engineering from the University of Patras, Greece, in 2006. He is a Professor in the School of Intelligent Systems Science & Engineering at Jinan University, China, affiliated with the University of Thessaly, Greece, and also Honorary Professor at Shandong Jiaotong University, China. His research interests fall into the broad areas of communication theory and wireless communications with emphasis on smart surfaces, optical wireless communications, non-orthogonal multiple access, and physical layer security.

Dr. Tsiftsis has served in the Editorial Boards of the IEEE TRANSACTIONS ON COMMUNICATIONS, IEEE TRANSACTIONS ON VEHICULAR TECHNOLOGY, and IEEE COMMUNICATIONS LETTERS. He is currently an Associate Editor of the IEEE Transactions on Wireless Communications and IEEE Transactions on Mobile Computing. Prof. Tsiftsis has been appointed as an IEEE Vehicular Technology Society Distinguished Lecturer (IEEE VTS DL) for two terms (2018-2022).